


RESEARCH

Open Access



A preclinical study on cell therapy as an adjunct to surgical decompression in degenerative cervical myelopathy via accelerating blood spinal cord barrier reconstitution and neurological recovery

Hyun Woo Kim¹, Liang Yu Shi¹, Min Goo Lee¹, Ra Hye Kim¹, Zhi Yi Fan¹, Paul Aarne Koljonen¹ and Graham Ka Hon Shea^{1*} 

Abstract

Background Degenerative cervical myelopathy (DCM) is the most common disorder affecting the cervical spinal cord in the developed world. Whilst surgery is effective, many patients suffer from residual neurological deficits post-decompression. Cell-based therapies have been studied for traumatic spinal cord injury models but not DCM and may be efficacious as an adjunct to surgical decompression via trophic factor secretion, parenchymal engraftment and/or blood spinal cord barrier reconstitution.

Methods 98 SD rats at age 10–12 weeks underwent five weeks of cervical compression by inserting a water-absorbent polyurethane polymer at the C4 epidural space or received sham surgery. Decompression surgery was performed by removing the polymer. Treatment groups received BM-MSCs (bone marrow-derived marrow stromal cells) or BM-neurospheres intravenously or intracisternally at the time of decompression. Locomotor function (BBB testing, rotarod testing, Forelimb Score, and Hind Limb Score) and blood-spinal cord barrier (BSCB) recovery via Evans blue extravasation was observed in 35 rats during the 10-week post-decompression recovery period. 30 rats were used to determine in vivo cell distribution and comparative efficacy of intravenous (IV) or intracisternal (CIS) injection. The remaining rats were sacrificed to assess for the engraftment of transplanted cells. In vivo bioluminescent imaging (BLI) of EGFP-Luciferase BM-MSCs localized cells grossly to organ systems, whilst immunohistochemistry (IHC) of spinal cord specimens targeting anti-human antigens facilitated localization at the site of compression.

Results BSCB disruption indicated by Evans Blue dye extravasation peaked at Week-4 post-decompression (DW4) and correlated with endoglin expression. Locomotor recovery after polymer removal was delayed with minor improvements observed by Week-8 post-decompression (DW8). IV and CIS injection of BM-MSCs did not lead to significant improvement in locomotor function ($p = 0.101$, Rotarod Test: PBS vs. CIS) nor of BSCB reconstitution by

*Correspondence:
Graham Ka Hon Shea
gkshea@hku.hk

Full list of author information is available at the end of the article



© The Author(s) 2025. **Open Access** This article is licensed under a Creative Commons Attribution-NonCommercial-NoDerivatives 4.0 International License, which permits any non-commercial use, sharing, distribution and reproduction in any medium or format, as long as you give appropriate credit to the original author(s) and the source, provide a link to the Creative Commons licence, and indicate if you modified the licensed material. You do not have permission under this licence to share adapted material derived from this article or parts of it. The images or other third party material in this article are included in the article's Creative Commons licence, unless indicated otherwise in a credit line to the material. If material is not included in the article's Creative Commons licence and your intended use is not permitted by statutory regulation or exceeds the permitted use, you will need to obtain permission directly from the copyright holder. To view a copy of this licence, visit <http://creativecommons.org/licenses/by-nc-nd/4.0/>.

Day 10 post-decompression. BLI showed significant peripheral organ entrapment of IV BM-MSCs, while CIS BM-MSCs remained in the cervical region, with IHC demonstrating localization to the pia mater. At Day 20, both CIS BM-MSCs and BM-neurospheres similarly failed to significantly improve locomotor function ($p=0.136$, Rotarod Test: PBS vs. BM-neurospheres) and transplanted cells were absent from the cervical cord parenchyma.

Conclusion Human BM-MSCs and BM-neurospheres demonstrate limited efficacy as adjunct therapy to cervical decompression under the present experimental conditions. Adjusting insertable polymer hardness, cell number, and timing of cell transplantation may be future means to demonstrate potential therapeutic effectiveness.

Keywords Degenerative cervical myelopathy, Blood-spinal cord barrier, Cervical decompression, Cell therapy, Bone marrow-derived marrow stem cells, Bone marrow-derived neurospheres

Background

Degenerative cervical myelopathy (DCM) is the most prevalent form of cervical spinal cord dysfunction in the developed world [1]. Incidence of hospitalization due to DCM is estimated to be 4.04 per 100,000 and rising due to the aging population [2]. DCM is characterized by progressive narrowing of the cervical spinal canal, typically caused by degenerative disc disease, thickening of the spinal ligaments, osteophyte formation, and can be exacerbated by occupational hazards or life-style habits involving repetitive flexion and extension of neck [3, 4]. Surgical decompression offers the best treatment outcomes, however recovery to near normal function (mJOA ≥ 16) declines sharply with DCM severity [5, 6]. Non-operative treatment modalities are largely ineffective in halting disease progression [7].

Blood-spinal cord barrier (BSCB) disruption is a key pathological factor in DCM and correlates with disease severity [8–10]. BSCB disruption by reperfusion injury likely occurs post-decompression in patients with moderate to severe DCM, hindering neurological recovery [11–14]. AlbuminQ, a clinical metric of BSCB integrity measured by the calculating the ratio of CSF: serum albumin concentration, is significantly increased in DCM, but largely stabilizes after cervical decompression [9, 10]. Nevertheless, albuminQ is more accurately a measure of blood-CSF barrier integrity and may not capture BSCB compromise at the capillaries where Virchow-Robin spaces are sealed [15]. Direct evidence of BSCB disruption in rodent DCM models may be demonstrated by significant blood Evans Blue dye (EBD) extravasation into the spinal/ cord parenchyma, however the extent of EBD leakage post-decompression in disease models remains unknown [16, 17].

Marrow stromal cells (MSCs) are now understood to possess a capacity to function as adventitial or perivascular cells in vivo, which support the blood-CNS barrier, facilitate vascular remodeling, and possess multipotency [18–24]. In the context of acute SCI, in vivo neurogenesis or gliogenesis by bone marrow (BM)-derived MSCs were found to be limited regardless of transplantation route,

thus its efficacy is now largely attributed to its trophic, angiogenic, and immunomodulatory properties [25–30].

Neurospheres were first described and cultured by Reynolds and Weiss to select and expand neural stem cells (NSCs) from neurogenic niches [31]. It was later discovered that neurospheres could be generated under similar culture conditions from BM-MSCs as well [32], and that human BM-derived neurospheres harbor neural crest-like stem cells capable of neuronal differentiation [33]. Comparative evaluation of rat BM-NSCs vs. subventricular zone-NSCs demonstrated that both NSC sources share analogous function and neuronal differentiation potential [34]. In animal SCI studies, transplanted BM-neurospheres showed lack of long-term survival after engraftment and differentiated mostly towards oligodendrocytes and astrocytes, not neurons [35–37].

Cell therapy interventions have yet to be tested in DCM, despite its widespread prevalence and the persistence of neurological deficits after surgery. Unlike traumatic SCI, DCM is characterized by stepwise progressive deterioration and from a clinical standpoint, there remains ample time for harvest and preparation of cells for transplantation. Here, we hypothesized that transplantation of BM-MSCs and BM-neurospheres may be useful to improve histological and neurological outcomes following decompression, in a rat implantable polymer model.

Methods

Research aim

This study was conducted to evaluate post-decompression locomotor recovery and BSCB reconstitution in an implantable polymer-induced degenerative cervical myelopathy (DCM) rat model. In addition, BM-MSC and BM-neurosphere were investigated as a therapeutic adjunct to surgical decompression by assessing its effect on locomotor recovery, BSCB reconstitution, and cellular migration and engraftment. All experiments were conducted at The University of Hong Kong, Faculty of Medicine, Laboratory Block. The work has been reported in line with the ARRIVE guidelines 2.0.

Insertable polymer rat DCM model

We utilized the insertable polymer rat DCM model as it replicates chronic progressive cervical cord progression characteristic of human DCM with relative ease and consistency whilst allowing for surgical decompression via polymer removal [38–40]. In this study, 10–12-week-old Sprague Dawley (SD) rats were used, with male and female rats utilized in separate experimental groups to avoid gender being a confounding factor. Meloxicam (1 mg/kg) was delivered one day before surgery via drinking water, whilst buprenorphine (0.1mL, 300 µg/mL) was administered subcutaneously 30 min prior to surgery. Anesthesia was delivered with isoflurane inhalation (5% induction) followed by intraperitoneal (IP) injection of ketamine (75–100 mg/kg) and xylazine (10 mg/kg). Surgical procedures were performed based on protocols described by Li et al. (2023) and Karadimas et al. (2013), with modifications [16, 17]. In brief, a 4-cm mid-line skin incision was made from cervical level 2 (C2) to thoracic level 2 (T2). Muscle and connective tissues were retracted to expose the vertebral column. C3–5 laminae were identified by counting spinous processes from C2. Ligamentum flavum at C3/4 was removed to expose the underlying dura. Next, the polyurethane polymer (2 mm x 1 mm x 1 mm, length x width x thickness, Guangzhou Fischer Chemical Co., Ltd., Guangzhou, China) was implanted into the C4 epidural space posterior to the cervical cord to induce compression. Polymer dimensions were determined according to dimensions utilized in previous studies [38, 39, 41]. For the sham surgery group, only the ligamentum flavum at C3/4 was removed, without polymer implantation. For decompression surgery, C4 laminectomy was performed, followed by removing the exposed polyurethane polymer. Thoroughness of decompression was confirmed by visual observation for dural sac pulsation.

Humane endpoint for euthanasia was determined with the following criteria: (1) incapable of feeding or drinking independently, (2) complete tetraplegia, or (3) loss of weight exceeding 20% of initial body weight prior to cervical compression or decompression surgery. Rats meeting any one of these criteria were euthanized with sodium pentobarbital overdose (120 mg/kg, i.p.).

Evans blue extravasation assay

Evans Blue dye (EBD) extravasation was used to study BSCB disruption in DCM rats [42]. 4% EB (206334, Sigma-Aldrich) solution was prepared in 0.9% saline solution and intravenously injected via the tail vein (2mL/kg) whilst rats were anaesthetized with isoflurane gas (5% induction, 2% maintenance). Rats were placed back into the cage after recovery. Six hours later, rats were euthanized with pentobarbital sodium overdose and transcardiac perfusion was performed with ice-cold PBS.

After complete perfusion, the cervical spinal cord from C2 - C7 was extracted. For ex vivo fluorescence quantification, Perkin Elmer In Vivo Imaging System– Spectrum (PE-IVIS) was used to visualize and quantify EBD extravasation at the cervical spinal cord (excitation / emission wavelengths: 620/680 nm, filter: 605/680 nm, exposure: 1 s, height: 0.5 cm). For each spinal cord, regions of interest (roi) of the same length and width were placed so that the point of highest EBD signal was placed at the center of the roi. For spectroscopic quantification, the C3 - C5 spinal cord was placed in 50% TCA solution in 1:3 weight (mg): volume (µL) ratio. Each cord was homogenized manually with a stainless-steel pestle for 5 min and centrifuged at 10,000 × g for 20 min. 40µL of the supernatant was mixed with 65µL of 95% ethanol per well in a 96-well microplate and its fluorescence emission (excitation/emission: 620/680 nm) was measured with CLARIOstar Plus. EBD concentrations were determined against a standard curve.

Behavioral tests

Rats were categorized as suffering from mild, moderate, and severe DCM based on their rotarod performance at Week 5 post-compression (female rats, severe: 0–24 s, moderate: 25–64 s, and mild: ≥ 65 s; male rats: severe: 0–14 s, moderate: 15–44 s, mild: ≥ 45 s). Mild, moderate, and severe DCM rats were randomly and evenly distributed to different interventional groups to control for the confounding effect of injury severity. Stratified randomization was performed with a random number generator with each group assigned a number. All behavioral tests were performed by blinded experimenters and blinded experimenters did not participate during animal grouping.

Rotarod test

A rotating rod (LE8306, Panlab) was used to assess balance and coordination. Briefly, each rat was placed on an accelerating spinning rotor (starting RPM: 15, end RPM: 50, total run time: 5 min) and allowed to run without falling for as long as possible. The Rotarod Test was performed five times per rat with 5 min breaks in-between. The three longest runtimes were recorded and averaged. Rats were trained with five runs per day for three days before the first measurement, and for subsequent tests, a single training session (five runs) was conducted the day prior.

Locomotor scoring test

The BBB (Basso, Beattie and Bresnahan) Locomotor Test, modified BBB (mBBB) test for cervical spinal cord injury, Forelimb Score (FLS), and Hind Limb Score (HLS) were used to assess locomotor function of rats [43, 44]. Each rat was placed on a black wooden round

table (radius = 60 cm) and allowed to move freely for up to 10 min. Locomotor function was evaluated independently by two blinded experimenters using the mBBB, BBB, FLS, and HLS scoring matrices. The final score for each test was the average of the two experimenters' assessments. Scoring matrices can be found in Table S1–S2 in Additional File 1.

Magnetic resonance imaging

MRI assessment of rats was carried out at the Laboratory of Biomedical Imaging and Signal Processing (BISP), University of Hong Kong, using a 7T MRI scanner (ParaVision v5.1, PharmaScan 70/16, Bruker Biospin GmbH, Germany). Rats were oriented in a prone position on a plastic holder with physiological monitoring using MRI-compatible sensors (SA Instruments, NY). The surface receiver coil was fixed in place directly above the cervical spinal cord. RARE T2-weighted images were acquired in sagittal planes with the following parameters: echo time: 12.962 ms, repetition time: 1672.766 ms, field-of-view: 40 mm x 40 mm, resolution: 156.25 μ m x 156.25 μ m, number of excitations: 1, acquisition time: 36 s, slice thickness: 1.0 mm, and number of slices: 12. Transverse plane images were acquired with the following parameters: echo time: 12ms, repetition time: 4200 ms, field-of-view: 32 mm x 32 mm, resolution: 125 μ m x 125 μ m, number of excitations: 2, acquisition time: 4 min 28 s, slice thickness: 1.0 mm, number of slices: 12.

BM-MSC and BM-neurosphere culture

Bone marrow was obtained from consenting donors requiring long bone reaming and intramedullary nailing from the Department of Orthopaedics and Traumatology, Queen Mary Hospital, Hong Kong, with ethics approval obtained from the Institutional Review Board of The University of Hong Kong / Hong Kong West Cluster (Study No. UW 10–157). BM-MSCs were selected by plastic adherence followed by subculture and expansion in 6-well plates (Greiner Bio-One) with BM-MSC medium, defined as Minimum Essential Medium α (Gibco) supplemented with 15% fetal bovine serum (ExCell Bio). BM-MSC cultures were maintained with medium change every two days and passaged at 1:3 following TrypLE (Invitrogen) dissociation. At Passage 4 or 5, BM-MSCs were tested for tri-lineage differentiation (see Fig. S1 in Additional File 1 for culture protocols), used for cell transplantation, or differentiated into BM-neurospheres.

BM-neurosphere culture was performed as previously described [45]. After passage 4–5, confluent BM-MSCs were dissociated with TrypLE and seeded at 3×10^5 cells per well in Ultra-Low Attachment Surface Polystyrene 6-well plates (Corning) in Neurosphere-Induction Medium (NIM). NIM was defined as Advanced

DMEM/F-12 (Gibco) supplemented with B27 (Invitrogen), 2mM GlutaMax (Gibco), 20ng/mL bFGF (Peprotech), and 20ng/mL EGF (Gibco). BM-neurospheres were maintained in NIM for eight to ten days. BM-neurosphere dissociation was performed with Accutase (Invitrogen) according to manufacturer instructions on Day 3–4 and 7–8. For transplantation studies, nascent BM-neurospheres were used (diameter = 10–50 μ m) as larger spheres could cause occlusion upon injection or require enzymatic dissociation prior to transplantation.

RNA sequencing

BM-MSCs and BM-neurospheres were cultured from bone marrow obtained from three consenting donors. RNA extraction was performed with NucleoSpin RNA (Macherey-Nagel) at passage 5 for BM-MSCs and at Day 9–10 for BM-neurospheres. Prior to sequencing, ribosomal RNA depletion was performed using QIAseq FastSelect–rRNA HMR Kit (Qiagen). cDNA libraries were prepared using KAPA RNA HyperPrep Kit (Roche). 500 ng of total RNA was used as starting material for ribosomal RNA depletion. Cytoplasmic rRNA, mitochondrial rRNA were removed by the QIAseq FastSelect reagents during NGS library preparation. The processed RNA was fragmented to 200–300 bp in the presence of magnesium ions. The fragmented rRNA-depleted RNA was applied as templates to synthesize first strand cDNA by using random hexamer-primers and reverse transcriptase. For second strand cDNA synthesis, the mRNA template was removed, and a replacement strand was generated to form blunt-end double-stranded (ds) cDNA. ds cDNA underwent, 3' adenylation and indexed adaptor ligation. The adaptor-ligated libraries were enriched by 12 cycles of polymerase chain reaction (PCR). Illumina NovaSeq 6000 was used for Pair-End 151 bp sequencing.

RNAseq data analysis

Raw sequencing reads were assessed for quality using FastQC and trimmed using Trimmomatic to remove adapters and low-quality sequences. Processed reads were then aligned to the genome using STAR, a splice-aware aligner, with GENCODE v35 as the reference annotation for accurate alignment of exonic and intronic regions. Gene-level quantification was performed using featureCounts. Differential expression analysis was performed using the DESeq2 algorithm [46] with prefiltering of genes (minimal count = 10, minimal sample size = 3). Log fold shrinkage was applied (apeglm method). Ensemble IDs were converted to gene symbols using the EnsDb.Hsapiens.v79 database [47]. Principal component analysis (PCA) was performed after regularized log data transformation, and volcano plots made with EnhancedVolcano [48]. Upregulated and downregulated Gene Ontology (GO) terms in BM-neurospheres (vs. BM-MSC) were

determined with gene set enrichment analysis (GSEA), after ascribing gene ranks ($-\log_{10}(\text{p-value}) \times \text{sign of fold change}$) to each differentially expressed gene. With a gene list of upregulated genes ($\text{padj} > 0.01$, $\log_2\text{fold-change} > 1$), GO network analysis was performed with ClueGO in Cytoscape with the following parameters: GO-term p-value threshold: 0.001, GO tree interval: 6–13, minimum number and % genes: 4 and 19.5 kappa score: 0.2. Several GO terms were removed to improve visibility of the GO Term network. Neurosphere markers [49–53], chemokine receptor genes [54–56], and pericyte markers [57, 58] were chosen from a selection of prior studies.

Intracisternal and intravenous injections

Intracisternal injection at the time of decompression was carried out as described by Mahat (2012) with modifications [59]. In brief, rats were anesthetized with isoflurane (5% induction, 2% maintenance) and placed in a stereotaxic frame (model 68528, RWD Life Sciences), secured with ear bars. The head was tilted at a flexed position and the injection site identified by palpation of the posterior limit of the magnum foramen and C1 vertebrae. A 31-gauge catheterized needle was inserted transcutaneously below the posterior limit of the magnum foramen into the cisterna magna. While inserting the needle, gentle negative pressure was maintained, and insertion was halted upon successful penetration into the cisterna magna confirmed by the withdrawal of clear cerebrospinal fluid. A 50 μL cell suspension of either BM-MSCs or BM-neurospheres (750,000 cells in PBS) was slowly injected at a rate of 20 $\mu\text{L}/\text{sec}$. After injection, the needle was kept in place for 1 min to prevent backflow. For intravenous injection, rats were anesthetized with isoflurane (5% induction, 2% maintenance). The tail was cleansed with 70% ethanol, and the lateral tail vein was identified. A 25-gauge needle was inserted into the tail vein near the tip of the lateral vein as evidenced by a flash of blood in syringe. 1 mL of cell suspension (BM-MSC only, 2×10^6 cells in αMEM) was injected at a rate of 100 $\mu\text{L}/\text{sec}$. Cell doses for intracisternal and intravenous injections were with accordance to dosing of MSCs previously used in the rat SCI model (range of 1×10^5 to 5×10^6) whilst the median cell count for intravenous delivery was 1×10^5 MSCs (ranging from 1×10^3 to 9×10^6) [60]. Given the robust safety profile of intravenous MSC injections reported in the literature and the limited data available for intracisternal administration, the intracisternal dose was conservatively chosen, whereas the intravenous dose was set higher.

EGFP-Luc BM-MSCs

To generate enhanced green fluorescence protein– luciferase expressing BM-MSCs, P1 BM-MSCs were cultured

at 30% confluency and transduced with lentiviral vector (rLV-EF1a-Luciferase-P2A-EGFP-T2A-Puro-WPRE, BrainVTA). P1 BM-MSCs were cultured in BM-MSC medium ($\alpha\text{MEM} + 15\%$ FBS) containing 50 $\mu\text{g}/\text{mL}$ protamine sulfate (P4020, Sigma-Aldrich) and lentiviral vectors at 10 multiplicity of infection (moi). After 24 h, BM-MSC medium was changed to $\alpha\text{MEM} + 15\%$ FBS and cells cultured until 70% confluency. Positive selection was performed via addition of 5 $\mu\text{g}/\text{mL}$ puromycin (Gibco) for 48 h. BM-MSCs were cultured in $\alpha\text{MEM} + 15\%$ FBS until Passage 5 and injected either intravenously or intracisternally into DCM rats.

In vivo bioluminescent imaging (BLI)

Rats that received EGFP-Luc BM-MSCs underwent BLI to track in vivo cell migration of BM-MSCs. Prior to BLI, rats were anesthetized with intraperitoneal (IP) injection of ketamine (75–100 mg/kg) + xylazine (10 mg/kg). Animals then received fresh luciferin solution (15 mg/mL in PBS, Revvity) intraperitoneally at 10 μL per gram of body weight. After 15 min, the rat was placed inside the PE-IVIS imaging chamber in a prone position and BLI was performed (open filter, exposure: auto, height: 3.5 cm). Cell migration was calculated by dividing the total flux (radiance) at the cervical spinal cord by total flux measured across the whole body.

Ex vivo cell migration

Immediately prior to cell injection, BM-MSCs and BM-neurospheres were labelled with Vybrant™ DiD Cell-Labeling Solution (Invitrogen) according to manufacturer instructions. At post-injection Day 20, euthanasia was performed with pentobarbital sodium overdose followed by transcardiac perfusion with 4% PFA. The vertebral column and skull were extracted and submerged in 4% PFA solution for one day and 30% sucrose solution for two days. The fixed brain and spinal cord were removed from the vertebral column and skull. To track the migration of DiD-labelled BM-MSCs and BM-neurospheres, ex vivo imaging of the brain and spinal cord was performed with PE-IVIS (excitation /emission: 648/670nm - DiD, filter: 640/680nm, exposure: 7 s, height: 0 cm). Migration Rate (% MR) was calculated by dividing the total fluorescence at the decompression site by total fluorescence measured across the brain and spinal cord.

Immunohistochemistry and immunocytochemistry

In preparation for immunohistochemistry (IHC), the rat brain and spinal cords were extracted after transcardiac perfusion, fixed in 4% PFA, and placed in 30% sucrose solution for three days. Samples were frozen in tissue freezing medium (Leica), cryosectioned, and mounted onto glass slides (J1800AMNZ, fisher scientific). For immunocytochemistry (ICC), BM-MSCs were cultured

on removeable chamber slides. Cyrosectioned tissue or cultured BM-MSCs were fixed in 4% PFA for 15 min and incubated in Blocking Buffer for 2 h at room temperature. Primary antibody staining was performed overnight at 4 °C in Antibody Dilution Buffer. For intracellular and nuclear markers, samples were additionally permeabilized with 0.3% PBST for 10 min prior to blocking. Afterwards samples were incubated with secondary antibody in Antibody Dilution Buffer for two hours. Nuclear staining was performed with 0.1% Hoechst 33,342 (Invitrogen) in PBS for 10 min at room temperature. Glass coverslips were placed on top of the tissue or cell samples with Mounting Medium (50001, Ibidi) and cells / sections imaged with an LSM780/880 confocal microscope (Zeiss). A complete list of buffer recipes and antibody list and catalogue number can be found in Table S3-S5 in Additional File 1.

Fluorescence quantification

ZEISS ZEN desk software was used to analyze fluorescence data from IHC. For mean fluorescence intensity (FI/um²) quantification, sum FI was divided by total spinal cord area (um²). Spinal cord area was defined by spline contour function traced around the DAPI-stained tissue region. Lower thresholds for the sum of FI was set specific to each marker studied to remove background noise. For co-localization quantification, ZEN desk co-localization function was used to derive the Pearson's co-localization coefficient (*r*) between two markers of interest. Co-localization coefficient (*r*) denotes the correlation of fluorescence intensity distribution between two markers. Co-localization coefficient (*r*) of ± 1.0 indicates perfect positive or negative linear co-localization correlation, while $r=0$ indicates no correlation. % Co-localization is defined as percentage of co-localizing pixels of each marker of interest. For selecting high-DiD regions to be imaged, each high-DiD spinal cord region was numbered and randomly selected with a random number generator.

Sample size calculation and statistical analysis

Minimal sample size per group for control-treatment experiments was determined by using the following formula: $n = 2\sigma^2(Z_{\alpha/2} + Z_{\beta})^2 / \Delta^2$ (Additional File 1, Figure S2). Δ FLS values (FLS: DW2 - CW5) for each rat in the pilot batch ($n=5$) shown in Fig. 1C were used to calculate standard derivation (σ). Minimum detectable difference (Δ) was set as 1.5, a conservative estimate from +3.9 in BBB score conferred by cell therapy in the context of traumatic SCI [60]. Since there are no prior studies examining cell therapy as an adjunct therapy to cervical decompression in DCM, cell therapy efficacy from a meta-analysis of traumatic SCI studies were used to estimate minimum detectable difference [56]. With $\sigma=1$,

$\Delta=2$, $Z_{\alpha}=1.96$, and $Z_{\beta}=0.8416$, n was determined to be at least 7 (6.977). Thus, initial samples sizes in all groups were set at $n=9-11$ to account for sample loss due to dropout. The number of rats that underwent DCM or sham surgery for each experiment was as follows: DCM progression ($n=8$), MRI ($n=4$), Evans Blue extravasation assay ($n=23$), PE-IVIS ($n=6$), intravenous vs. intracisternal BM-MSC ($n=24$), and BM-MSC vs. BM-neurosphere ($n=33$), with a total of $n=98$. Sample size estimation for Evans Blue extravasation experiment was not possible due to lack of prior studies investigating progressive changes in BSCB permeability post-cervical decompression in rodents and was set as $n=6$. Sample sizes for MRI and PE-IVIS studies were minimal ($n=1$ for MRI and $n=3$ for PE-IVIS) as they were pilot experiments.

All statistical analysis was performed on GraphPad Prism 10.2.3. Paired one-way or two-way ANOVA analysis were performed, unless specified otherwise. P-values were taken to be statistically significant at <0.05 . Power analysis for pooled analysis (Fig. 7) was conducted using the formula: $N = \{(r+1) (Z_{\alpha/2} + Z_{1-\beta})^2 \sigma^2\} / d^2$ ($r=n1/n2$ ratio of sample size, σ =pooled standard deviation, d =difference of means of two groups, $Z_{1-\beta}=0.84$ for power 0.8, $Z_{\alpha/2}=1.96$ for alpha 0.5). Mean values and SD values from all experimental groups are shown in graphical representation (error bar = σ).

Results

Locomotor recovery and BSCB reconstitution are delayed after cervical decompression

Female SD rats were divided into two groups- DCM group ($n=5$), who received the implantable polymer, and sham surgery control group ($n=3$) to characterize the progressive changes in locomotor function post-cervical compression and decompression. DCM model illustration and the schedule for neurological assessment is shown in Fig. 1A-B. After 5-weeks post cervical compression, FLS, HLS, and body weight decreased significantly, and FLS & HLS remained low compared to baseline (Fig. 1C). Post-decompression improvement in locomotor function was delayed with significant improvement observed at DW8 and DW10 in HLS and FLS, respectively. Significant improvement in rotarod performance post-decompression was not observed ($p=0.246$). Separately, four female SD rats underwent DCM surgery (5-week compression, followed by decompression via polymer removal) and T2-weighted MRI scans of the cervical spinal cord were conducted on mild, moderate, and severe DCM rats to document for radiological compression (Fig. 1D). DCM severity was determined by rotarod performance (severe: 0–25 s, moderate: 25–65 s, and mild: > 65 s).

To assess the extent of BSCB disruption post-decompression, a total of 19 female SD rats underwent DCM

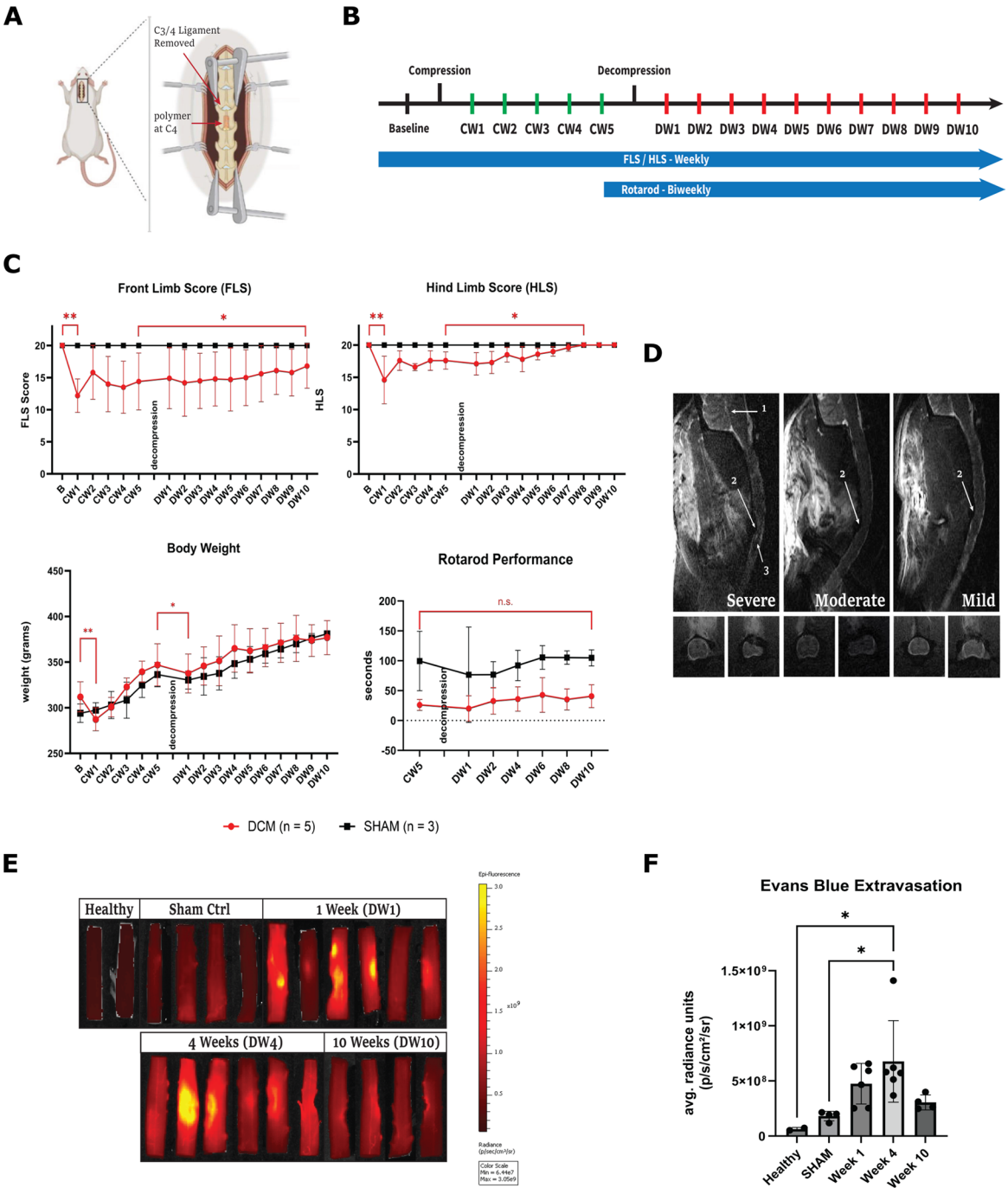


Fig. 1 DCM disease model and blood-spinal cord barrier characterization. **(a)** For cervical compression, the ligamentum flavum at C3/4 was surgically removed and a polyurethane sheath (2 mm x 1 mm x 1 mm, LxWxH) inserted at the exposed C4 epidural space. **(b)** Timeline of conducted behavioral experiments. The duration of cervical compression and post-decompression recovery was 5 weeks and 10 weeks, respectively. (CW1 = post-cervical compression Week 1, DW1 = post-cervical decompression Week 1) **(c)** Results for behavioral tests and body weight changes over time. **(d)** T2-weighted MRI scans of rat spinal cords at DW1 for severe, moderate, and mild DCM. Top panels shows sagittal MRI scans (left– dorsal, right– ventral, top– cranial, bottom– caudal) of each rat spinal cord. Axial spinal cord images on the bottom left and right of each sagittal image correspond to the adjacent inferior non-compressed spinal cord and the most severely compressed spinal cord region, respectively. Arrow 1 marks the hindbrain, arrow 2 marks the decompression site, and arrow 3 marks T2-hyperintensity. **(e)** EBD extravasation at DW1, DW4, and DW10 demonstrated by ex vivo epifluorescence images of cervical spinal cords **(f)** EBD extravasation quantified by average radiance units (photons/sec/cm²/steradian) within each spinal cord’s compressed region

surgery, with the EBD extravasation assay performed at Week 1 ($n=6$), Week 4 ($n=6$), and Week 10 ($n=4$) post-decompression. DCM dropout rate was 15.8% (humane endpoint reached: $n=2$, surgical complications: $n=1$). EBD measurements were conducted at DW1 for sham control group ($n=4$). To visualize and quantify EBD extravasation, each spinal cord was harvested and imaged ex vivo with PE-IVIS (Fig. 1E-F). Elevated EBD extravasation was seen in DW1 (+262.1%), DW4 (+373.9%), and DW10 (+168.4%) compared to sham control, but only reached statistical significance at DW4 ($p=0.0251$). From these results it could be inferred that BSCB permeability peaked around DW4, and by DW10 was nearly reconstituted.

Evans blue extravasation co-localizes with VEGF and endoglin, not MMP9

The extent of BSCB damage, reperfusion-induced oxidative stress, and vascular remodeling are critical factors that affect post-decompression neurological recovery in DCM [8, 61–63]. After ex vivo imaging, injured spinal cord regions from healthy ($n=1$), sham ($n=3$), DW1 ($n=3$), DW4 ($n=3$), and DW10 ($n=4$) were sectioned and stained to assess for the extent of BSCB breakdown (EBD and MMP9), oxidative stress (4HNE), acute inflammation (TNF α), glial scarring (CS56), and vascular remodeling (VEGF and endoglin) [64–71]. Each marker was imaged together with EBD to measure its co-localization to areas of BSCB breakdown. Spinal cord sections with negligible EBD extravasation were omitted from co-localization analysis.

Overall, marker elevation and BSCB breakdown were most apparent at DW1 and DW4 (Fig. 2A). Specifically, CS56 and 4HNE were expressed the most at DW1. EBD extravasation peaked at DW4, while VEGF and MMP9 remained similarly elevated at both DW1 and DW4. Among all six markers explored, endoglin expression was the most correlated with EBD extravasation. Figure 2B shows a heatmap of correlation coefficients between each marker against EBD FI measured across all samples, except the healthy group ($n=1$). Analysis for signal co-localization also demonstrated congruence between EBD with endoglin and VEGF signals ($r=0.455$ and $r=0.303$), but not with 4HNE, CS56, MMP9, and TNF α (Fig. 2C-D). This implied that EBD extravasation was consistent to regions with “active” CD105+ (endoglin) blood vessels undergoing vascular remodeling and vessel maturation, rather than in regions with acute BSCB breakdown (MMP9) as seen in acute SCI [66, 72–74].

Neurosphere induction of BM-MSCs upregulates neuronal pathways

RNAseq was performed on BM-MSCs and BM-neurosphere cultures from three donors (Patient 9, 12, and 15)

to investigate whether neuronal pathways and canonical neurosphere markers were upregulated after neurosphere induction (Fig. 3A-B). PCA results indicated a distinct gene expression profiles in BM-MSCs vs. BM-neurospheres, with minor sample variance between patients (Fig. 3C). Differential gene expression analysis revealed 1740 upregulated and 1449 downregulated genes in BM-neurospheres vs. BM-MSCs with $\text{padj}>0.01$ and $\log_2\text{foldchange}>1$ set as threshold (Fig. 3D). Full list of up- and down-regulated genes can be found in Additional File 2. Figure 3E shows top upregulated GO terms ranked by GSEA normalized enrich score (NES), which included terms linked to synapse components and functions, such as synaptic membrane and neurotransmitter receptor activity, as well as biological pathways associated with bone, cartilage, and CNS development. Figure 3F shows downregulated GO terms, which mostly comprised of terms associated with cellular division and proliferation. Additional File 3 contains the full list of enriched GO terms, as well as KEGG, Reactome, and WikiPathway terms. GO term network created with a separate list of upregulated genes with ClueGo (cytoscape) indicated a connection between CNS development and kidney development, with the latter further associated with WNT signaling, bone, and cartilage development pathways (Fig. 3G). As expected, neurosphere induction increased expression of neural stem cell markers such as GFAP, NGFR, and nestin, while changes in expression of fate-committed neuroglial markers (MAP2, NF200, MBP) were minimal (Fig. 3H). As shown in Fig. 3I, neurosphere induction also increased the expression of CXCR4 and CCR1, both key chemokine receptors involved in neural stem cell migration during development [75–77]. For pericyte markers in Fig. 3J, only genes associated with angiogenesis were upregulated (PECAM, PDGFRB, and VEGFA).

Both intracisternal and intravenous BM-MSCs did not significantly improve locomotor function nor attenuate Evans blue leakage

A total of 30 female SD rats underwent DCM surgery and were given either intravenous (IV) BM-MSCs ($n=12$), intracisternal (CIS) BM-MSCs ($n=10$), or PBS ($n=8$) to assess the migration and efficacy of IV and CIS BM-MSCs in the post-decompression DCM model. Experimental dropout rate was 13.3% (humane endpoint reached: $n=2$, surgical complications: $n=2$). Cells were delivered immediately after decompression surgery (CW5) and locomotor function was assessed at D10 (Day 10 post-decompression), followed by EBD extravasation assay on the same day (D10). For three rats ($n=3$) each in IV and CIS group, BM-MSCs used were transduced with EGFP-Luc containing lentiviral vector (EGFP-Luc BM-MSCs) to track in vivo distribution at D5 post-decompression.

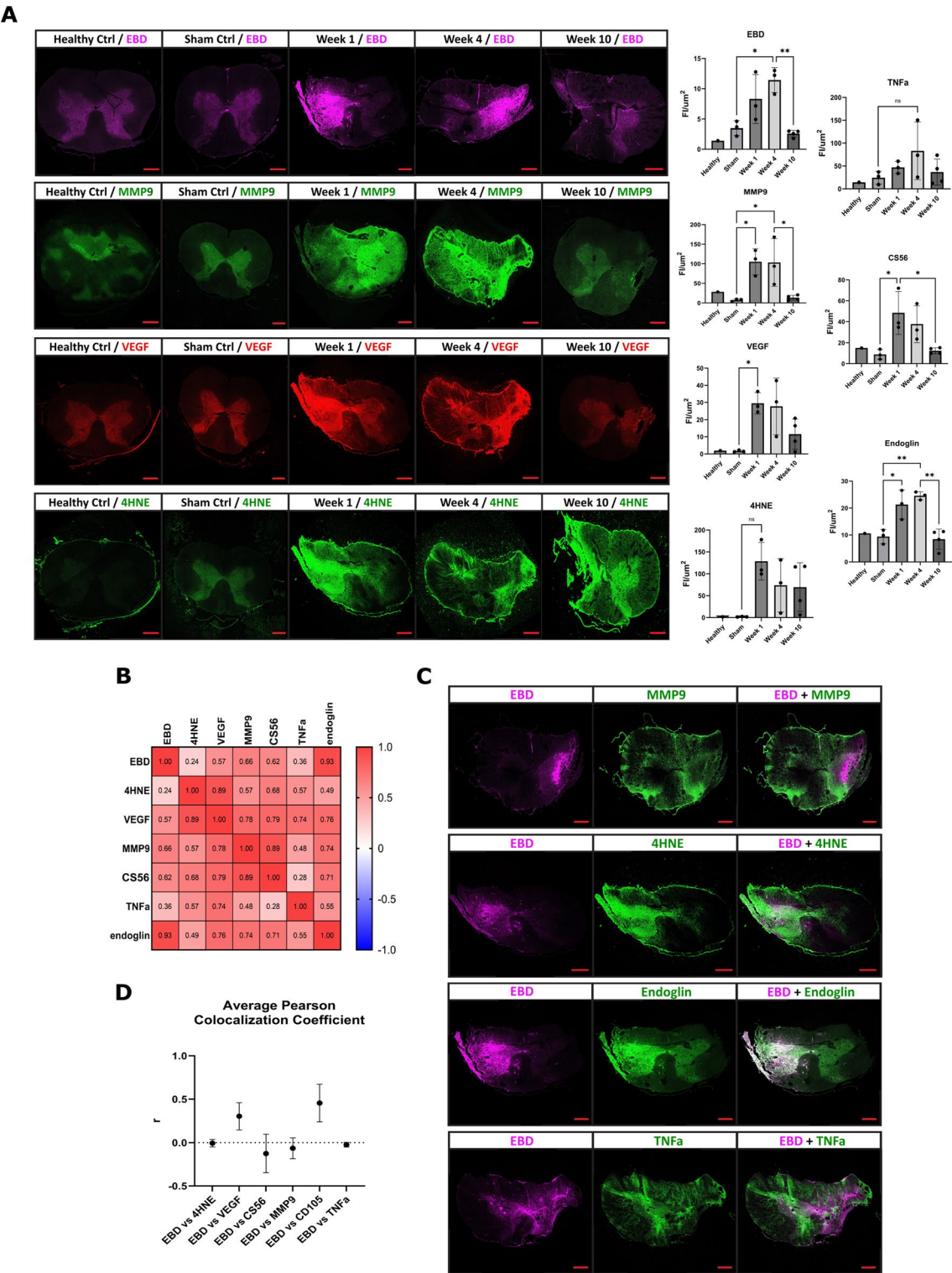


Fig. 2 Correlation of blood-spinal cord barrier reconstitution with cell lineage markers. **(a)** Average fluorescence intensity (FI) of extravasated EBD, MMP9, VEGF, and 4HNE in healthy, sham surgery, DW1, DW4, and DW10 compressed spinal cords (scale bar = 500 μ m). See Fig. S3–S5 in Additional File 1 for IHC images of TNF α , endoglin, and CS56 **(b)** Heatmap of Pearson correlation coefficient (r) of all markers in relation to EBD. Strong positive correlation was noted between FI of endoglin vs. EBD, MMP9 vs. CS56 (CSPG), and VEGF vs. 4HNE ($p < 0.001$). Weak correlation was observed between FI of EBD vs. 4HNE ($p = 0.422$), EBD vs. TNF α ($p = 0.226$), and CS56 (CSPG) vs. TNF α ($p = 0.348$). **(c)** Overlay images of EBD + MMP9, EBD + 4HNE, EBD + endoglin, EBD + TNF α (scale bar = 500 μ m). For EBD + endoglin, pseudo-coloring (red \rightarrow green) has been used for better visualization of co-localization. Co-localized areas are shaded in white. See Fig. S5 for IHC images of EBD + CS56 and EBD + endoglin

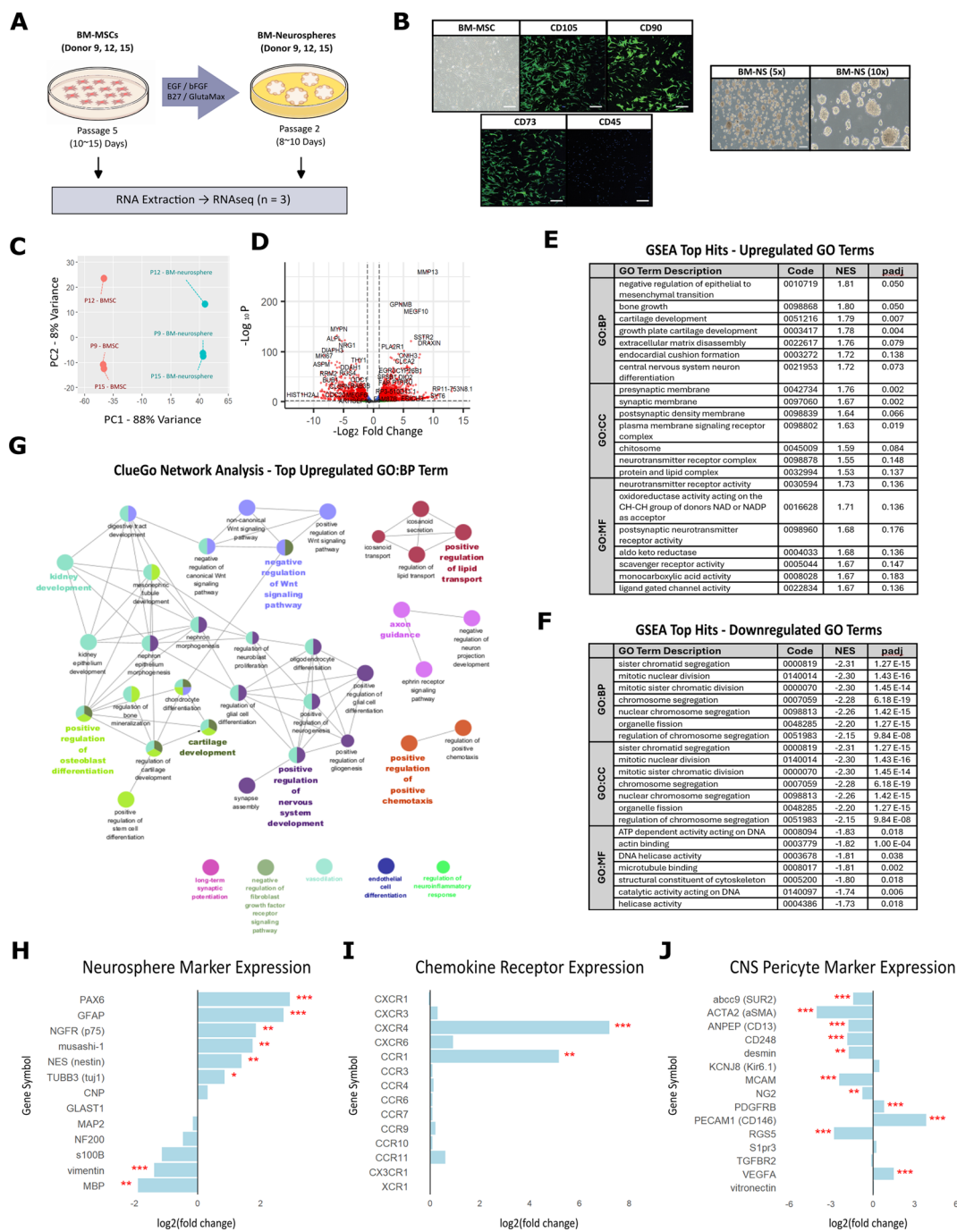


Fig. 3 Characterization of BM-MSCs and BM-Neurospheres. **(a)** RNAseq experiment design. **(b)** BM-MSC and BM-NS culture derivation and immunohistochemistry. BM-MSCs were plastic adherent, positive for MSC markers (CD105, CD90, CD73) and negative for CD45 (scale bar = 20 μm), whilst BM-neurospheres (Day 7) were generated in response to FGF and EGF (scale bar = 100 μm). **(c)** PCA plot made from P9, 12, and 15 BM-MSC and BM-neosphere after regularized log gene count transformation. **(d)** Volcano plot of significantly upregulated and downregulated genes shown in red (p -value < 0.01, $\log_2\text{foldchange}$ > 1). **(e)** Upregulated GO: BP, GO: CC, and GO: MF terms ranked by GSEA NES score. **(f)** Downregulated GO: BP, GO: CC, and GO: MF terms ranked by GSEA NES score. **(g)** ClueGO network analysis made of highly associated GO: BP terms (P < 0.001) with upregulated genes. Nodes indicate individual GO: BP terms, whilst edges between nodes indicate significant overlap of associated genes (κ score > 0.2). GO: BP terms with > 50% shared genes are grouped and labelled by the GO: BP term with the lowest p -value. **(h-j)** Key neurosphere, chemokine receptor, and CNS pericyte marker differential gene expression in BM-neurospheres vs. BM-MSCs (* = p -value < 0.05, ** = p -value < 0.01, *** = p -value < 0.001)

Rats given EGPF-Luc BM-MSCs were omitted from behavioral tests and the EBD extravasation assay.

Post-decompression locomotor recovery, measured by change (D10 - CW5) in FLS, rotarod performance, and body weight, did not improve significantly with CIS or IV BM-MSc intervention (Fig. 4A). CIS group showed +12.4 s improvement in rotarod performance at D10 compared to CW5 (-32 s), but did not reach significance (CIS:ΔRotarod vs. PBS:ΔRotarod, $p=0.101$). EBD extravasation measured by both PE-IVIS and microplate spectroscopy showed that neither CIS nor IV BM-MSc injections attenuated EBD leakage by D10 (Fig. 4B-C). Increase in EBD extravasation correlated negatively with Δ FLS, indicating that rats with poorer outcomes after decompression had more BSCB disruption (Fig. 4D). The same trend was not observed in Δ rotarod ($p=0.301$) as shown in Fig. 4E. Entrapment of EGPF-Luc BM-MSCs in peripheral organs was significant in the IV group, whilst luminescence signal was largely detected only at the cervical and lumbar spinal cord region for the CIS group (Fig. 4F). Due to the proximity of the injection site to the injury site, it was difficult to ascertain whether CIS injected EGPF-Luc BM-MSCs mostly remained at the cisterna magna or migrated to the injured spinal cord region, or both. IV vs. CIS % migration did not reach significance due to large variance in CIS group, possibly due to lower N number ($n=3$) and variability in luciferin absorption rate and cell survival (Fig. 4G).

Both intracisternal BM-MSc and BM-neurosphere did not significantly improve locomotor function by D20 post-decompression

33 male rats underwent DCM surgery and received PBS ($n=9$), BM-MSCs ($n=11$), or BM-neurospheres ($n=10$) intracisternally to determine its migration rate and in vivo differentiation. DCM dropout rate was 9.1% (humane endpoint reached: $n=3$). Cell injection was performed at the time of decompression and locomotor function was assessed at D10 and D20. Four rats from the BM-MSc ($n=4$) and BM-neurosphere ($n=4$) groups received DiD-marked cells to enable cell tracing with ex vivo fluorescence imaging and immunohistochemistry, performed upon sacrifice at D20.

None of the measured neurological outcomes (BBB, mBBB, FLS, and rotarod) showed significant improvement from baseline across all groups (Fig. 5A). Post-decompression locomotor recovery measured at D10 and D20 was not significantly improved by CIS BM-MSCs or BM-neurospheres, compared to PBS control. By D20, rotarod performance improved the most in the BM-MSc group (+2.1 s, CW5=26.8 s, D10=28.9 s) but did not reach significance vs. PBS group ($p=0.136$). BM-MSc and BM-neurosphere groups showed similar distribution to each other throughout the spinal cord

with fluorescence intensity concentrated at the injection site and hindbrain (Fig. 5B). Cell migration, quantified by average fluorescence signal intensity at the compression site, did not differ significantly between BM-MSCs vs. BM-neurospheres (Fig. 5C). Both groups had little to no presence of DiD+ cells at the injury site and human nuclei immunopositivity was not observed throughout the spinal cord parenchyma (Fig. 5D-E).

DiD + BM-MSc and BM-neurospheres co-localized with S100β, but not CD146 or NeuN

At endpoint (D20), spinal cords of rats receiving DiD-labelled BM-MSCs ($n=4$) or BM-neurospheres ($n=4$) were retrieved and stained for perivascular (CD146), glial (S100β), and neuronal markers (NeuN) together with DiD (Fig. 6A-B). Spinal cord regions to be imaged were randomly selected to comprise of three high-DiD signal regions per spinal cord section (Fig. 6C). Co-localization analysis indicated most DiD+ cells were S100β+, likely astrocytes or oligodendrocytes positioned near the meninges, while contribution to the perivascular niche (CD146+) and to neuronal progeny (NeuN+) was low.

Behavior data from all animal experiments were pooled and locomotor recovery after cervical decompression measured by Δ FLS (D10– CW5) and Δ Rotarod (D10– CW5). Pooled analysis shown in Fig. 7A-B indicated no significant difference in locomotor recovery post-decompression between male vs. female rats (ΔFLS p -value=0.094, Δrotarod p -value=0.753, t -test). Post-decompression improvement in rotarod performance was significantly higher in severe DCM rats compared to mild or moderate DCM rats as shown in Fig. 7C-D (p value=0.003 and 0.004, respectively). Rats across all disease severity groups show limited change in FLS and rotarod performance by cell therapy intervention with none reaching statistical significance when compared to matched PBS control (Fig. 7E-F). Power analysis results on pooled rotarod data (PBS vs. Treatment) indicated at least 35 animals were required per treatment arm to achieve 80% power ($\alpha=0.05$) for significant improvement in motor testing, indicating a large locomotor outcome variability for the current disease model and treatment paradigm.

Discussion

To the best of our knowledge, this work represents the first attempt to investigate cell therapy as an adjunct to surgical decompression in a rodent model of DCM. Whilst the polymer implantation method is relatively established, limitations affecting model performance and reproducibility should be understood in the context of other available models. Five different types of DCM animal models have been used in experimental studies as outlined by Kanbara et al. (Table 1) [39]. The

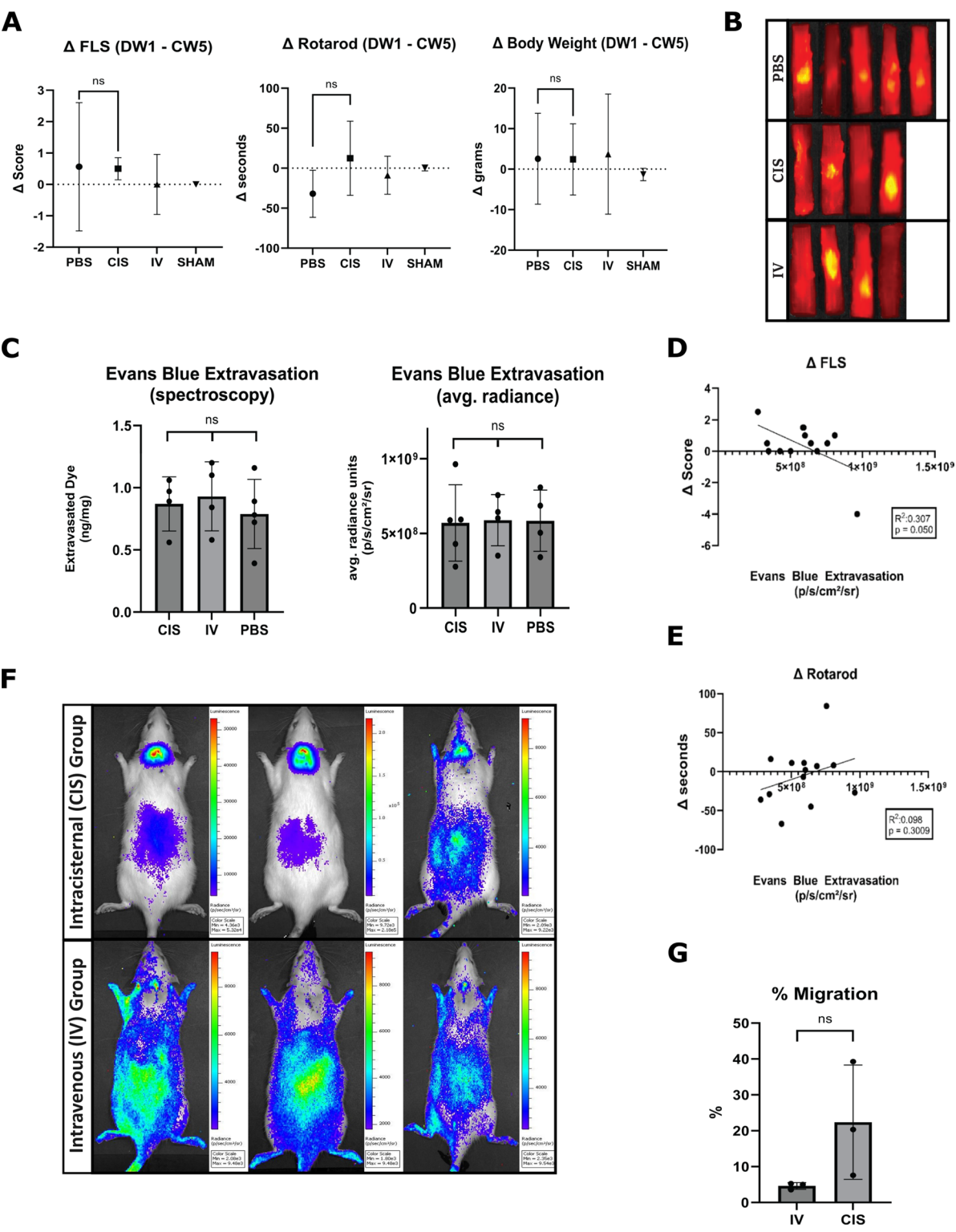


Fig. 4 Blood brain barrier reconstitution post-transplantation. **(a)** Post-decompression outcomes (FLS, rotarod performance, and body weight) shown by change at Day 10 (D10) from baseline (CW5). **(b)** In vivo distribution of EGPF-Luc BM-MSCs injected via IV vs. CIS. **(c)** Average percent migration following IV vs. CIS delivered cells calculated by bioluminescence in cervical spinal cord vs. whole body x 100%. **(d)** EBD extravasation at D10 for CIS, IV, and PBS treatment groups. **(e)** EBD extravasation quantified by PE-IVIS (average radiance) and microplate spectroscopy (ng / mg of spinal cord tissue). **(f-g)** Correlation graphs of EBD extravasation measured by PE-IVIS versus Δ FLS and Δ rotarod

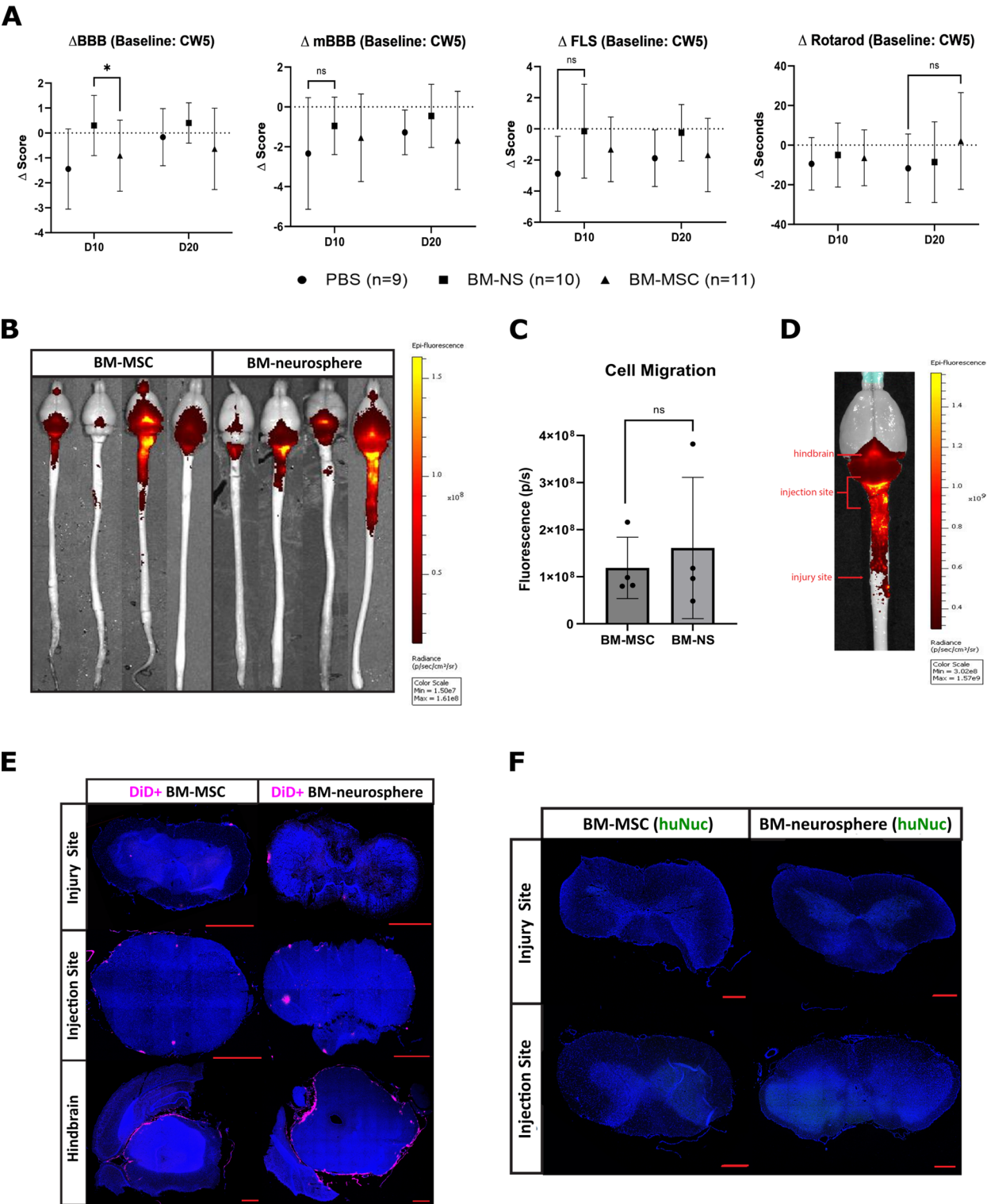


Fig. 5 Neurological function and localization of cells at post-transplantation. **(a)** FLS, mBBB, BBB, and Rotarod Test performance of DCM rats at CW5, Day 10 (D10) and D20 post-decompression. Change (Δ) in score or performance for each test at D10 and D20 is represented with respect to performance at CW5. **(b-c)** Ex vivo fluorescence imaging of DiD-labelled BM-MSCs and BM-neurospheres at D20. Cell migration to the injured region as shown in (c) was measured using PE-IVIS with roi selection. T-test was performed to compare migration between BM-MSCs vs. BM-neurospheres. **(d)** Magnified and labelled (hindbrain, injection site, and injury site) ex vivo fluorescence image as well as **(e-f)** spinal cord immunohistochemical sections at injury site, injection site, and hindbrain. **(e)** DiD+ cells were mostly located at the meninges (scale bar = 1000 μ m). **(f)** Results after staining for human nuclei (HuNuc) at injury site and injection site also showing an absence of transplanted cells within the cord parenchyma (scale bar = 500 μ m)

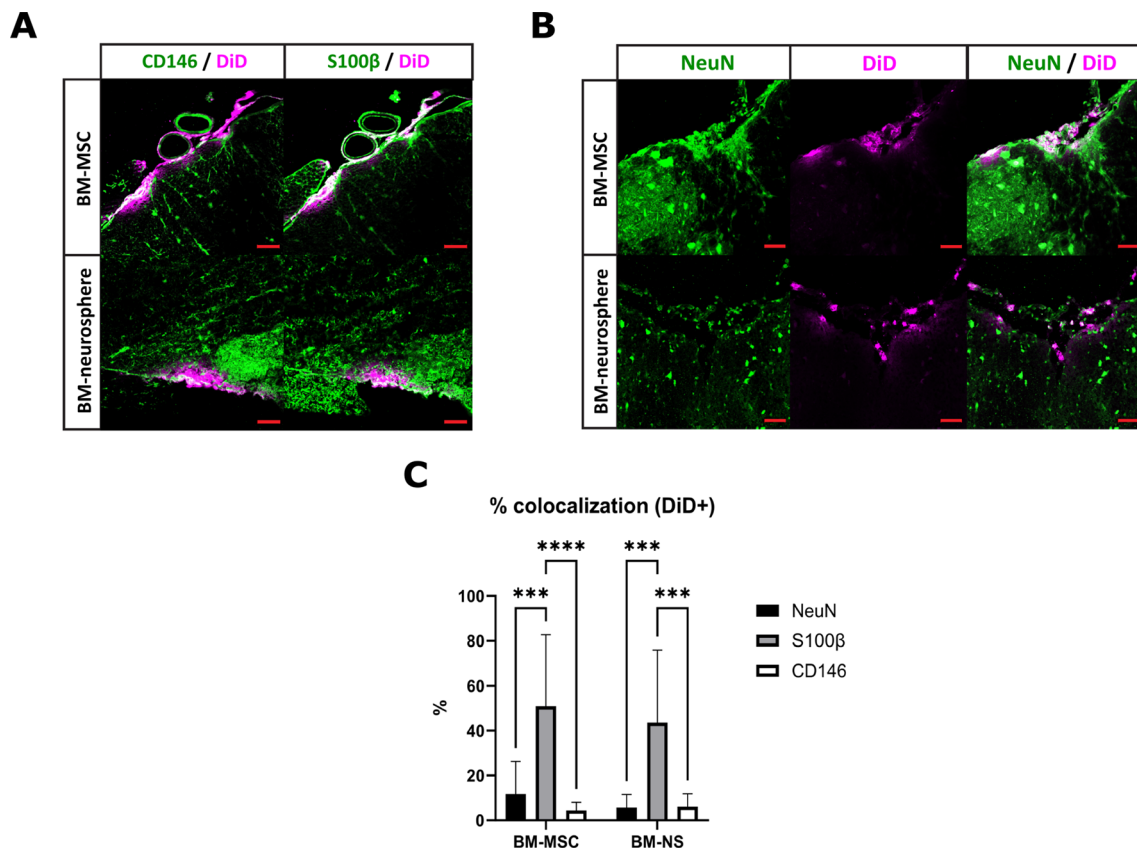


Fig. 6 Characterizing cell fate of transplanted cells. **(a)** Representative images of DiD+ BM-MSCs and BM-neurosphere co-localization with CD146 and S100β. Pseudocoloring (CD146: Red → Green) was used for better visualization of co-localization. **(b)** Representative images of DiD+ BM-MSC and BM-neurosphere co-localization with NeuN. **(c)** % Co-localization of DiD signal with NeuN, S100β, and CD146

water-absorbing polyurethane polymer model, as was used in our study, demonstrated evidence of subacute injury upon polymer insertion (seen in CW1– FLS and HLS) and the absence of persistent and slowly progressive deterioration typical of human pathology. As recommended by Ijima et al., harder polymer material (such as AquapreneDx) may be used in future work to overcome such limitations [16, 38, 41]. Interestingly, modulating the expansion rate or the thickness of soft, but not hard, polyurethane polymer had negligible impact on the disease pathology or progression of DCM [38, 41].

BSCB disruption is increasingly recognized as a pathological event in traumatic and degenerative neurological conditions including DCM [8]. This likely occurs by four distinct mechanisms and contexts in DCM– (1) Primary injury caused by direct physical compression, (2) Hypoxia-induced BSCB hyper-permeability in mildly ischemic spinal cord regions, (3) BSCB disruption from post-decompression reperfusion injury, and (4) Elevated BSCB permeability during revascularization of compressed regions after decompression [8, 16]. Another novel contribution of our work was to extensively document BSCB breakdown and reconstitution in the rat DCM model, both with and without receiving cell

therapy. We observed that EBD extravasation peaked at Week 4 post-decompression, likely a result of increased angiogenesis and vascular remodeling as high-EBD regions co-localized with VEGF and endoglin, and not as a the sequelae of post-decompression reperfusion injury which often occurs from 1 to 3 days post-decompression [14, 62, 83]. Vascular regeneration and neuroprotection are some of the key therapeutic mechanisms provided by transplanted MSCs [84], but our results demonstrated a failure in the BM-MSC group to reduce EBD extravasation by D10. For comparison, human BMSCs delivered intravenously 1 h after cervical SCI in rats led to a reduction in EBD extravasation as early as Day 1 [85]. Similarly rapid BSCB reconstitution ability was observed upon SCI models receiving rat BMSCs [86–88].

Consistent to prior reports, cells delivered intravenously demonstrated significant entrapment in peripheral organs, while cells introduced intracisternally mostly remained at the injection site and hindbrain but were not specifically localized to the compressed spinal cord region [89–91]. Several studies have indicated robust injury site migration and parenchymal penetration of BM-MSCs delivered via lumbar puncture into the CSF, whilst others concurred with our results in reporting

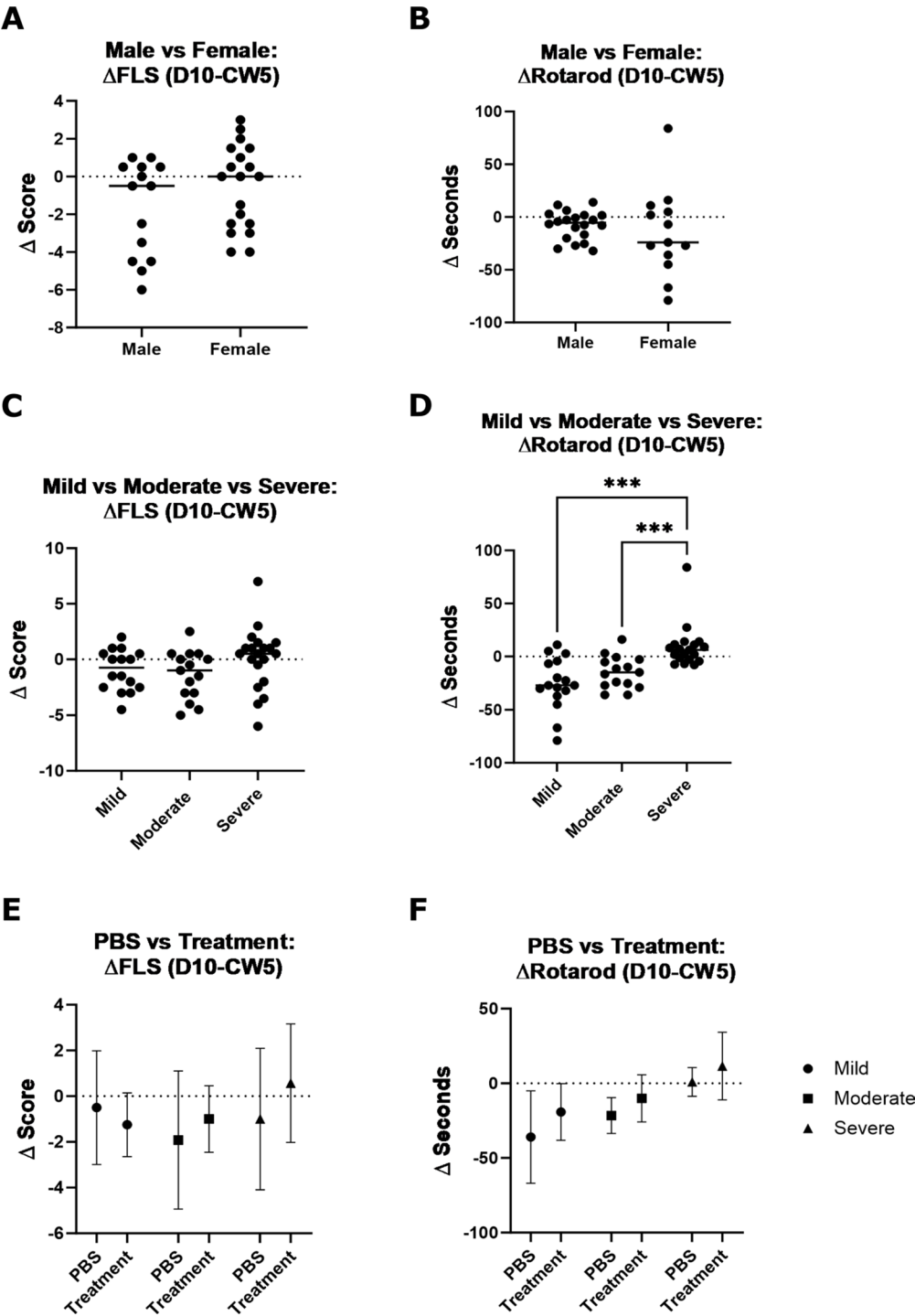


Fig. 7 Analysis of neurological outcomes across treatment subgroups. **(a-b)** Δ FLS and Δ Rotarod of male vs. female rats with each rat matched for disease severity and experimental group. **(c-d)** Δ FLS and Δ Rotarod of mild vs. moderate vs. severe DCM rats with each rat matched by sex and experimental group. **(e-f)** Δ FLS and Δ Rotarod of PBS vs. treatment group with rats matched by sex and disease severity

that cells remained only at the meningeal layers, without engraftment into the spinal cord parenchyma [26, 28, 92]. The discrepancy in findings may be attributed to differences in timing and dosing regimen of cellular delivery, as one study adopted repeated BM-MSCs injections at

Day 7, 8, and 9 following SCI and demonstrated engraftment of BM-MSCs into the damaged white matter. On the contrary, a single dose of cellular transplantation inject at Day 3 or repetitive injections at Day 3, 4, and 5 found BM-MSCs to be present at the pia mater only [93,

Table 1 Rodent DCM models

DCM Model	Description	Advantages	Disadvantages	References
twy-twy mice model	Gradual cervical spinal cord compression by genetic ossification of the posterior longitudinal ligament and ligamentum flavum	Reproducible rate of deterioration that mimics step-wise neurological deterioration of DCM	-Development of joint ankylosis complicates motor tests - Site of maximal compression different to human pathology	[78, 79]
Polyethylene thread model	Polyethylene thread is tied around the cervical spinal column, restricting the natural axial growth of the spinal cord	-No surgical operation required on the spinal cord - Chronic compression and late onset neurological decline reflects natural history of DCM	-Takes 6 to 9 months (in rats) to develop symptoms	[80]
Titanium-screw model	Cervical laminectomy followed by insertion of a titanium screw overlying the dura	-Enables fine control over spinal cord compression	-Invasive surgical procedure	[81]
Polyether sheet model	Gradual thickening and calcification of the inserted aromatic polyether compresses the cervical spinal cord	-Chronic, slowly progressive compression by gradual calcification	-Lack of accessibility to the polymer material	[11, 17, 82]
Water-absorbing polyurethane polymer model	Insertion of gradually expanding water-absorbent polyurethane polymer at the cervical spinal cord	-Compression can be standardized with identical thickness and swell rate of the polymer	-Acute spinal cord injury upon insertion -Variable results based on polymer material	[38, 39]

94]. These relate to the concept of a transplantation window when the spinal cord is more receptive to cells after the acute cytotoxic inflammatory response has attenuated, thus numerous studies suggest that administering MSCs during the subacute phase (Days 7–9) and at high doses ($\geq 1 \times 10^6$) with repeated injections yields are means to achieve enhanced migration profiles, integration into injured white matter, and greater promotion of axonal sprouting and remyelination [94–96]. Overall, our results failed to demonstrate that adjunct cell therapy could improve neurological outcomes. Optimal transplantation parameters should be investigated in the context of the rat DCM model before the potential for therapeutic application is ruled out.

The prevailing mechanisms by which MSCs facilitate neural regeneration include immunomodulation, promotion of axonal outgrowth, and vascular repair, mediated via the secretion of signaling and growth factors [84]. The post-engraftment fate of MSCs remains unclear, but several studies indicate engraftment as pericyte-like cells [22, 97, 98]. This pericyte-like phenotype underlies their reported effects on reconstituting the BBB/BSCB [99]. Our results, however, did not show a reduction in Evans Blue extravasation by intravenous or intracisternal MSC injection and showed a lack of engraftment. In fact, our results of increased Evans Blue leakage during post-decompression may have been more representative of increased angiogenesis and revascularization rather than BSCB breakdown. For neural stem cells (NSC), the proposed mechanisms of action following transplantation include replacement of neuronal and glial populations in addition to trophic factor secretion, although in vivo effects vary depending on culture conditions and progenitor identity [100, 101]. Neurosphere culture induces NSCs to adopt an astrocyte-like undifferentiated

state upon transplantation with increased proliferative and self-renewal capacity [102]. When BM-MSCs are cultured under neurosphere-forming conditions, mesenspheres result which can self-renew, express NSC markers, and differentiate into neuronal and glial-like phenotypes in vitro [103]. Our RNAseq results substantiate upregulation of key NSC markers and pathways, and our recent integrative scRNAseq analysis revealed that Nestin⁺ PDGFR α ⁺ BM-MSCs within long bone marrow originates from the neural crest and may be biased towards neuronal differentiation [104]. Nevertheless, intracisternal transplantation of BM-neurospheres in the DCM animal model resulted in cells remaining at the pia mater; cells did not migrate and engraft into the injured spinal cord parenchyma nor give rise to neurons and glia.

Limitations to this study include polymer performance, which could not fully replicate the slowly progressive deterioration of DCM in human subjects and was subject to variability between experimental animals. Optimization of polymer material and size, as well as a longer observational period for both BSCB and neurological recovery would be means for future improvement [105]. Optimization of cell transplantation dosing and timing would also be essential. Based on the meta-analysis of cell therapy in various animal models of SCI, a high dose of stem cells ($\geq 1 \times 10^6$) and transplantation at the subacute phase (3–14 days post-SCI) may be ideal [106]. Repeating xenograft experiments with immunosuppressants such as cyclosporin A could reduce immunorejection as a confounder for lack of efficacy, although others have demonstrated that immunosuppression is not required to demonstrate efficacy of human MSC transplantation in SCI and various CNS injury rodent models [93, 105, 107–110].

Conclusion

In a water-absorbing polymer DCM rat model, post-decompression locomotor recovery was delayed with significant improvement observed by Week 8 post-decompression. Extensive spinal cord EBD extravasation continued up to 4-weeks post-cervical decompression and likely resulted from vascular remodeling, rather than breakdown of the BSCB. Results from this study did not demonstrate evidence for the efficacy of BM-MSCs and BM-neurospheres as an adjunct therapy for cervical decompression. Further optimization of the disease model, cell dosing and timing are required.

Abbreviations

BBB Score / Test	Basso, Beattie and Bresnahan locomotor score / test
BBB	blood-brain barrier
BLI	in vivo bioluminescent imaging
BM-MSCs	bone marrow-derived marrow stromal cells
BM-neurosphere	bone marrow-derived neurosphere
BSCB	blood-spinal cord barrier
CIS	intracisternal injection
CW1	post-compression week 1
DCM	degenerative cervical myelopathy
DW1	post-decompression week 1
EBD	Evans blue dye
FLS	forelimb score
HLS	hindlimb score
IHC	immunohistochemistry
ISCT	International Society of Cell & Gene Therapy
IV	intravenous injection
mBBB	modified BBB
PE-IVIS	Perkin Elmer in vivo imaging system-- spectrum
SCI	spinal cord injury

Supplementary Information

The online version contains supplementary material available at <https://doi.org/10.1186/s13287-025-04348-9>.

Supplementary Material 1
Supplementary Material 2
Supplementary Material 3
Supplementary Material 4

Acknowledgements

The authors acknowledge the assistance of the University of Hong Kong Li Ka Shing Faculty of Medicine Faculty Core Facility and Centre for Comparative Medicine Research (CCMR) for assisting with animal husbandry and veterinary services. Facilities and staff at the Laboratory of Biomedical Imaging and Signal Processing were also essential for data collection. The authors also acknowledge University of Hong Kong Li Ka Shing Faculty of Medicine Centre for PanorOmic science for performing sample processing, library preparation, and RNA sequencing services. The authors declare that they have not used AI-generated work in this manuscript in this section.

Author contributions

H. Kim, L. Shi, and P. Koljonen wrote the manuscript. H. Kim and L. Shi have planned and executed the experiments. R. Kim, M. Lee, and Z. Shi have assisted in data collection. G. Shea has supervised the project and revised the manuscript. All authors read and approved the final manuscript.

Funding

'Get Up and Walk Campaign' awarded to PA Koljonen.

Data availability

All data generated or analyzed during this study are included in this published article and its Additional Files 2–4.

Declarations

Ethics approval and consent to participate

All animal experiments were performed under the animal license issued by the Department of Health, Hong Kong. Animal experimental procedures were reviewed and approved by Committee on the Use of Live Animals in Teaching and Research (CULATR), The University of Hong Kong (no. 22–258). Title: Pericyte Transplantation and Chondroitinase ABC Enzyme Injection for a Rat Model of Degenerative Cervical Myelopathy. Date of approval: November 1st 2022. Collection of BMSCs from human subjects were reviewed and approved by the Institutional Review Board of the Hospital Authority / Hong Kong West Cluster (no. UW 19–040). Title: Harnessing human bone marrow-derived neural crest progenitors for regenerative medicine. Date of approval: January 28 2019.

Consent for publication

Not applicable.

Competing interests

None to declare.

Author details

¹Department of Orthopaedics and Traumatology, LKS Faculty of Medicine, The University of Hong Kong, Hong Kong, China

Received: 30 January 2025 / Accepted: 15 April 2025

Published online: 28 May 2025

References

1. Nouri A, Cheng JS, Davies B, Kotter M, Schaller K, Tessitore E. Degenerative Cervical Myelopathy: A Brief Review of Past Perspectives, Present Developments, and Future Directions. *J Clin Med* [Internet]. 2020;9(2):535. Available from: <https://pubmed.ncbi.nlm.nih.gov/32079075>
2. Nouri A, Tetreault L, Singh A, Karadimas SK, Fehlings MG. Degenerative Cervical Myelopathy: Epidemiology, Genetics, and Pathogenesis. *Spine (Phila Pa 1976)* [Internet]. 2015;40(12):E675–93. Available from: <https://pubmed.ncbi.nlm.nih.gov/25839387/>
3. Milligan J, Ryan K, Fehlings M, Bauman C. Degenerative cervical myelopathy: diagnosis and management in primary care. *Can Fam Physician*. 2019;65(9):619–24.
4. Baptiste DC, Fehlings MG. Pathophysiology of cervical myelopathy. *The Spine Journal* [Internet]. 2006;6(6):S190–7. Available from: <https://doi.org/10.1016/j.spinee.2006.04.024>
5. Tetreault LA, Karadimas S, Wilson JR, Arnold PM, Kurpad S, Dettori JR et al. The Natural History of Degenerative Cervical Myelopathy and the Rate of Hospitalization Following Spinal Cord Injury: An Updated Systematic Review. *Global Spine J* [Internet]. 2017;7(3 Suppl):285–345. Available from: <https://pubmed.ncbi.nlm.nih.gov/29164030>
6. Fehlings MG, Tetreault LA, Kurpad S, Brodke DS, Wilson JR, Smith JS et al. Change in Functional Impairment, Disability, and Quality of Life Following Operative Treatment for Degenerative Cervical Myelopathy: A Systematic Review and Meta-Analysis. *Global Spine J* [Internet]. 2017;7(3 Suppl):535–69S. Available from: <https://pubmed.ncbi.nlm.nih.gov/29164033>
7. Fehlings MG, Tetreault LA, Riew KD, Middleton JW, Wang JC. A Clinical Practice Guideline for the Management of Degenerative Cervical Myelopathy: Introduction, Rationale, and Scope. *Global Spine J* [Internet]. 2017;7(3 Suppl):21S–27S. Available from: <https://pubmed.ncbi.nlm.nih.gov/29164027>
8. Kim HW, Yong H, Shea GKH. Blood-spinal cord barrier disruption in degenerative cervical myelopathy. *Fluids Barriers CNS* [Internet]. 2023;20(1):68. Available from: <https://pubmed.ncbi.nlm.nih.gov/37743487>
9. Blume C, Geiger MF, Brandenburg LO, Müller M, Mainz V, Kalder J et al. Patients with degenerative cervical myelopathy have signs of blood spinal cord barrier disruption, and its magnitude correlates with myelopathy severity: a prospective comparative cohort study. *European Spine Journal*

- [Internet]. 2020;29(5):986–93. Available from: <https://doi.org/10.1007/s00586-020-06298-7>
10. Schmidt TP, Jütten K, Bertram U, Brandenburg LO, Pufe T, Delev D et al. Blood spinal cord barrier disruption recovers in patients with degenerative cervical myelopathy after surgical decompression: a prospective cohort study. *Sci Rep* [Internet]. 2023;13(1):7389. Available from: <https://pubmed.ncbi.nlm.nih.gov/37149638>
 11. Karadimas SK, Laliberte AM, Tetreault L, Chung YS, Arnold P, Foltz WD et al. Riluzole blocks perioperative ischemia-reperfusion injury and enhances postdecompression outcomes in cervical spondylotic myelopathy. *Sci Transl Med* [Internet]. 2015;7(316). Available from: <https://doi.org/10.1126/scitranslmed.aac6524>
 12. Algahtani AY, Bamsallim M, Alghamdi KT, Alzahrani M, Ahmed J. Cervical spinal cord ischemic reperfusion injury: A comprehensive narrative review of the literature and case presentation. *Cureus*. 2022;14(9):e28715.
 13. Hasan W, Khan K, Alomani N. Cervical cord reperfusion injury: a rare complication of spine surgery. *Int J Emerg Med*. 2022;15(1):39.
 14. Vidal PM, Karadimas SK, Uldreaj A, Laliberte AM, Tetreault L, Forner S et al. Delayed decompression exacerbates ischemia-reperfusion injury in cervical compressive myelopathy. *JCI Insight*. 2017;2(11).
 15. Lam MA, Hemley SJ, Najafi E, Vella NGF, Bilston LE, Stoodley MA. The ultra-structure of spinal cord perivascular spaces: implications for the circulation of cerebrospinal fluid. *Sci Rep*. 2017;7(1):12924.
 16. Li GS, Chen GH, Wang KH, Wang XX, Hu XS, Wei B et al. Neurovascular Unit Compensation from Adjacent Level May Contribute to Spontaneous Functional Recovery in Experimental Cervical Spondylotic Myelopathy. *Int J Mol Sci* [Internet]. 2023;24(4):3408. Available from: <https://pubmed.ncbi.nlm.nih.gov/36834841>
 17. Karadimas SK, Moon ES, Yu WR, Satkunendrarajah K, Kallitsis JK, Gatzounis G et al. A novel experimental model of cervical spondylotic myelopathy (CSM) to facilitate translational research. *Neurobiol Dis* [Internet]. 2013;54:43–58. Available from: <https://doi.org/10.1016/j.nbd.2013.02.013>
 18. de Souza LEB, Malta TM, Kashima Haddad S, Covas DT. Mesenchymal stem cells and pericytes: to what extent are they related? *Stem Cells Dev*. 2016;25(24):1843–52.
 19. Sacchetti B, Funari A, Remoli C, Giannicola G, Kogler G, Liedtke S, et al. No identical mesenchymal stem cells at different times and sites: human committed progenitors of distinct origin and differentiation potential are incorporated as adventitial cells in microvessels. *Stem Cell Rep*. 2016;6(6):897–913.
 20. Kim S, Lee S, Lim J, Choi H, Kang H, Jeon NL, et al. Human bone marrow-derived mesenchymal stem cells play a role as a vascular pericyte in the reconstruction of human BBB on the angiogenesis microfluidic chip. *Biomaterials*. 2021;279:121210.
 21. Klein D. Vascular Wall-Resident multipotent stem cells of mesenchymal nature within the process of vascular remodeling: cellular basis, clinical relevance, and implications for stem cell therapy. *Stem Cells Int*. 2016;2016:1905846.
 22. Menezes K, Rosa BG, Freitas C, da Cruz AS, de Siqueira Santos R, Nascimento MA, et al. Human mesenchymal stromal/stem cells recruit resident pericytes and induce blood vessels maturation to repair experimental spinal cord injury in rats. *Sci Rep*. 2020;10(1):19604.
 23. Yang C, Li Z, Liu Y, Hou R, Lin M, Fu L, et al. Single-cell Spatiotemporal analysis reveals cell fates and functions of transplanted mesenchymal stromal cells during bone repair. *Stem Cell Rep*. 2022;17(10):2318–33.
 24. Chao YX, He BP, Tay SSW. Mesenchymal stem cell transplantation attenuates blood brain barrier damage and neuroinflammation and protects dopaminergic neurons against MPTP toxicity in the substantia nigra in a model of Parkinson's disease. *J Neuroimmunol*. 2009;216(1–2):39–50.
 25. Lee J, Kuroda S, Shichinohe H, Ikeda J, Seki T, Hida K et al. Migration and differentiation of nuclear fluorescence-labeled bone marrow stromal cells after transplantation into cerebral infarct and spinal cord injury in mice. *Neuropathology* [Internet]. 2003;23(3):169–80. Available from: <https://doi.org/10.1046/j.1440-1789.2003.00496.x>
 26. Mothe AJ, Bozkurt G, Catapano J, Zabojoja J, Wang X, Keating A et al. Intrathecal transplantation of stem cells by lumbar puncture for thoracic spinal cord injury in the rat. *Spinal Cord* [Internet]. 2011;49(9):967–73. Available from: <https://doi.org/10.1038/sc.2011.46>
 27. Novikova LN, Brohlin M, Kingham PJ, Novikov LN, Wiberg M. Neuroprotective and growth-promoting effects of bone marrow stromal cells after cervical spinal cord injury in adult rats. *Cytherapy* [Internet]. 2011;13(7):873–87. Available from: <https://doi.org/10.3109/14653249.2011.574116>
 28. Pal R, Gopinath C, Rao NM, Banerjee P, Krishnamoorthy V, Venkataramana NK et al. Functional recovery after transplantation of bone marrow-derived human mesenchymal stromal cells in a rat model of spinal cord injury. *Cytherapy* [Internet]. 2010;12(6):792–806. Available from: <https://doi.org/10.3109/14653249.2010.487899>
 29. Gu W, Zhang F, Xue Q, Ma Z, Lu P, Yu B. Transplantation of bone marrow mesenchymal stem cells reduces lesion volume and induces axonal regrowth of injured spinal cord. *Neuropathology* [Internet]. 2009;30(3):205–17. Available from: <https://doi.org/10.1111/j.1440-1789.2009.01063.x>
 30. Xia Y, Zhu J, Yang R, Wang H, Li Y, Fu C. Mesenchymal stem cells in the treatment of spinal cord injury: Mechanisms, current advances and future challenges. *Front Immunol* [Internet]. 2023;14:1141601. Available from: <https://pubmed.ncbi.nlm.nih.gov/36911700>
 31. Soares R, Ribeiro FF, Lourenço DM, Rodrigues RS, Moreira JB, Sebastião AM et al. The neurosphere assay: an effective in vitro technique to study neural stem cells. *Neural Regen Res* [Internet]. 2021;16(11):2229–31. Available from: <https://pubmed.ncbi.nlm.nih.gov/33818505>
 32. Kohyama J, Abe H, Shimazaki T, Koizumi A, Nakashima K, Gojo S, et al. Brain from bone: efficient meta-differentiation of marrow stroma-derived mature osteoblasts to neurons with Noggin or a demethylating agent. *Differentiation*. 2001;68(4–5):235–44.
 33. Changmeng Z, Hongfei W, Cheung MCH, Chan YS, Shea GKH. Revealing the developmental origin and lineage predilection of neural progenitors within human bone marrow via single-cell analysis: implications for regenerative medicine. *Genome Med* [Internet]. 2023;15(1):66. Available from: <https://pubmed.ncbi.nlm.nih.gov/37667405>
 34. Yang J, Yan Y, Ciric B, Yu S, Guan Y, Xu H et al. Evaluation of bone marrow- and brain-derived neural stem cells in therapy of central nervous system autoimmunity. *Am J Pathol* [Internet]. 2010;177(4):1989–2001. Available from: <https://pubmed.ncbi.nlm.nih.gov/20724590>
 35. Zhang Htian, Cheng Hyu, Cai Yqian, Ma X, Liu W, peng, Yan Z, jie et al. Comparison of adult neurospheres derived from different origins for treatment of rat spinal cord injury. *Neurosci Lett* [Internet]. 2009;458(3):116–21. Available from: <https://doi.org/10.1016/j.neulet.2009.04.045>
 36. Suzuki H, Taguchi T, Kato Y, Kanchiku T, Imagama T, Yara T et al. Transplantation of neurospheres derived from bone marrow stromal cells promotes neurological recovery in rats with spinal cord injury. *Med Mol Morphol* [Internet]. 2011;44(3):131–8. Available from: <https://doi.org/10.1007/s00795-010-0519-y>
 37. Parr AM, Kulbatski I, Tator CH. Transplantation of Adult Rat Spinal Cord Stem/Progenitor Cells for Spinal Cord Injury. *J Neurotrauma* [Internet]. 2007;24(5):835–45. Available from: <https://doi.org/10.1089/neu.2006.3771>
 38. Iijima Y, Furuya T, Koda M, Matsuura Y, Saito J, Kitamura M et al. Experimental rat model for cervical compressive myelopathy. *Neuroreport* [Internet]. 2017;28(18):1239–45. Available from: <https://pubmed.ncbi.nlm.nih.gov/28957944>
 39. Kanbara S, Ohkawara B, Nakashima H, Ohta K, Koshimizu H, Inoue T et al. Zonisamide ameliorates progression of cervical spondylotic myelopathy in a rat model. *Sci Rep* [Internet]. 2020;10(1):13138. Available from: <https://pubmed.ncbi.nlm.nih.gov/32753675>
 40. Xu J, Long H, Chen W, Cheng X, Yu H, Huang Y, et al. Ultrastructural features of neurovascular units in a rat model of chronic compressive spinal cord injury. *Front Neuroanat*. 2017;11:136.
 41. Long HQ, Li GS, Lin EJ, Xie WH, Chen WL, Luk KDK et al. Is the speed of chronic compression an important factor for chronic spinal cord injury rat model? *Neurosci Lett* [Internet]. 2013;545:75–80. Available from: <https://doi.org/10.1016/j.neulet.2013.04.024>
 42. Wang HL, Lai TW. Optimization of Evans blue quantitation in limited rat tissue samples. *Sci Rep* [Internet]. 2014;4:6588. Available from: <https://pubmed.ncbi.nlm.nih.gov/25300427>
 43. Basso DM, Beattie MS, Bresnahan JC. A sensitive and reliable locomotor rating scale for open field testing in rats. *J Neurotrauma*. 1995;12(1):1–21.
 44. Martinez M, Brezun JM, Bonnier L, Xerri C. A New Rating Scale for Open-Field Evaluation of Behavioral Recovery after Cervical Spinal Cord Injury in Rats. *J Neurotrauma* [Internet]. 2009;26(7):1043–53. Available from: <https://doi.org/10.1089/neu.2008.0717>
 45. Mung KL, Tsui YP, Tai EY, Chan YS, Shum DKY, Shea GKH. Rapid and efficient generation of neural progenitors from adult bone marrow stromal cells by hypoxic preconditioning. *Stem Cell Res Ther* [Internet]. 2016;7(1):146. Available from: <https://pubmed.ncbi.nlm.nih.gov/27717376>
 46. Love MI, Huber W, Anders S. Moderated Estimation of fold change and dispersion for RNA-seq data with DESeq2. *Genome Biol*. 2014;15(12):550.

47. Zhu A, Ibrahim JG, Love MI. Heavy-tailed prior distributions for sequence count data: removing the noise and preserving large differences. *Bioinformatics*. 2019;35(12):2084–92.
48. Blighe K, Rana S, Lewis M, EnhancedVolcano. Publication-ready volcano plots with enhanced colouring and labeling. 2018.
49. Tsui YP, Lam G, Wu KLK, Li MTS, Tam KW, Shum DKY et al. Derivation of oligodendrocyte precursors from adult bone marrow stromal cells for remyelination therapy. *Cells*. 2021;10(8).
50. Mukai T, Nagamura-Inoue T, Shimazu T, Mori Y, Takahashi A, Tsunoda H, et al. Neurosphere formation enhances the neurogenic differentiation potential and migratory ability of umbilical cord-mesenchymal stromal cells. *Cytotherapy*. 2016;18(2):229–41.
51. Gil-Perotin S, Duran-Moreno M, Cebrián-Silla A, Ramírez M, García-Belda P, García-Verdugo JM. Adult neural stem cells from the subventricular zone: a review of the neurosphere assay. *Anat Rec (Hoboken)*. 2013;296(9):1435–52.
52. Kabos P, Ehteshami M, Kabosova A, Black KL, Yu JS. Generation of neural progenitor cells from whole adult bone marrow. *Exp Neurol*. 2002;178(2):288–93.
53. Bossolasco P, Cova L, Calzarossa C, Rimoldi SG, Borsotti C, Deliliers GL, et al. Neuro-glial differentiation of human bone marrow stem cells in vitro. *Exp Neurol*. 2005;193(2):312–25.
54. Proudfoot AEI. Chemokine receptors: multifaceted therapeutic targets. *Nat Rev Immunol*. 2002;2(2):106–15.
55. Veevers-Lowe J, Ball SG, Shuttleworth A, Kielty CM. Mesenchymal stem cell migration is regulated by fibronectin through $\alpha 5 \beta 1$ -integrin-mediated activation of PDGFR- β and potentiation of growth factor signals. *J Cell Sci*. 2011;124(Pt 8):1288–300.
56. Baek SJ, Kang SK, Ra JC. In vitro migration capacity of human adipose tissue-derived mesenchymal stem cells reflects their expression of receptors for chemokines and growth factors. *Exp Mol Med*. 2011;43(10):596–603.
57. Smyth LCD, Rustenhoven J, Scotter EL, Schweder P, Fauli RLM, Park TH, et al. Markers for human brain pericytes and smooth muscle cells. *J Chem Neuroanat*. 2018;92:48–60.
58. Vanlandewijck M, He L, Mäe MA, Andrae J, Ando K, Del Gaudio F, et al. A molecular atlas of cell types and zonation in the brain vasculature. *Nature*. 2018;554(7693):475–80.
59. Mahat MYA, Fakruddeen Ali Ahamed N, Chandrasekaran S, Rajagopal S, Narayanan S, Surendran N. An improved method of transcutaneous cisterna magna puncture for cerebrospinal fluid sampling in rats. *J Neurosci Methods*. 2012;211(2):272–9.
60. Oliveri RS, Bello S, Biering-Sørensen F. Mesenchymal stem cells improve locomotor recovery in traumatic spinal cord injury: Systematic review with meta-analyses of rat models. *Neurobiol Dis* [Internet]. 2014;62:338–53. Available from: <https://doi.org/10.1016/j.nbd.2013.10.014>
61. Hu J, Yu Q, Xie L, Zhu H. Targeting the blood-spinal cord barrier: A therapeutic approach to spinal cord protection against ischemia-reperfusion injury. *Life Sci*. 2016;158:1–6.
62. Dong Q, Sun L, Peng L, Yan B, Lv J, Wang G, et al. Expression of C5a and its receptor following spinal cord ischemia reperfusion injury in the rat. *Spinal Cord*. 2015;53(8):581–4.
63. Shingu H, Kimura I, Nasu Y, Shiotani A, Oh-hama M, Hijioka A, et al. Microangiographic study of spinal cord injury and myelopathy. *Paraplegia*. 1989;27(3):182–9.
64. Paauiwe M, Heijkants RC, Oudt CH, van Pelt GW, Cui C, Theuer CP, et al. Endoglin targeting inhibits tumor angiogenesis and metastatic spread in breast cancer. *Oncogene*. 2016;35(31):4069–79.
65. Shibuya M. Vascular endothelial growth factor (VEGF) and its receptor (VEGFR) signaling in angiogenesis: A crucial target for Anti- and Pro-Angiogenic therapies. *Genes Cancer*. 2011;2(12):1097–105.
66. Noble LJ, Donovan F, Igarashi T, Goussev S, Werb Z. Matrix metalloproteinases limit functional recovery after spinal cord injury by modulation of early vascular events. *J Neurosci*. 2002;22(17):7526–35.
67. Ahuja CS, Wilson JR, Neri S, Kotter MRN, Druschel C, Curt A, et al. Traumatic spinal cord injury. *Nat Rev Dis Primers*. 2017;3:17018.
68. Luo F, Wang J, Zhang Z, You Z, Bedolla A, Okwubido-Williams F, et al. Inhibition of CSPG receptor PTPo promotes migration of newly born neuroblasts, axonal sprouting, and recovery from stroke. *Cell Rep*. 2022;40(4):11137.
69. Gao D, Zhang X, Jiang X, Peng Y, Huang W, Cheng G, et al. Resveratrol reduces the elevated level of MMP-9 induced by cerebral ischemia-reperfusion in mice. *Life Sci*. 2006;78(22):2564–70.
70. Jean WC, Spellman SR, Nussbaum ES, Low WC. Reperfusion injury after focal cerebral ischemia: the role of inflammation and the therapeutic horizon. *Neurosurgery*. 1998;43(6):1382–96. discussion 1396–7.
71. Guo C, Tong L, Xi M, Yang H, Dong H, Wen A. Neuroprotective effect of Calyculin on cerebral ischemia and reperfusion injury in rats. *J Ethnopharmacol*. 2012;144(3):768–74.
72. ten Dijke P, Goumans MJ, Pardali E. Endoglin in angiogenesis and vascular diseases. *Angiogenesis*. 2008;11(1):79–89.
73. Paczkowska E, Rogińska D, Pius-Sadowska E, Jurewicz A, Piecyk K, Safranow K, et al. Evidence for proangiogenic cellular and humoral systemic response in patients with acute onset of spinal cord injury. *J Spinal Cord Med*. 2015;38(6):729–44.
74. Remacle AG, Hullugundi SK, Dolcas J, Angert M, Chernov AV, Strongin AY, et al. Acute- and late-phase matrix metalloproteinase (MMP)-9 activity is comparable in female and male rats after peripheral nerve injury. *J Neuroinflammation*. 2018;15(1):89.
75. Knerlich-Lukoschus F, Krossa S, Krause J, Mehdorn HM, Scheidig A, Held-Feindt J. Impact of chemokines on the properties of spinal cord-derived neural progenitor cells in a rat spinal cord lesion model. *J Neurosci Res*. 2015;93(4):562–71.
76. Tran PB, Banisadr G, Ren D, Chenn A, Miller RJ. Chemokine receptor expression by neural progenitor cells in neurogenic regions of mouse brain. *J Comp Neurol*. 2007;500(6):1007–33.
77. Dziembowska M, Tham TN, Lau P, Vitry S, Lazarini F, Dubois-Dalcq M. A role for CXCR4 signaling in survival and migration of neural and oligodendrocyte precursors. *Glia*. 2005;50(3):258–69.
78. Hirai T, Uchida K, Nakajima H, Guerrero AR, Takeura N, Watanabe S et al. The prevalence and phenotype of activated microglia/macrophages within the spinal cord of the hyperostotic mouse (twy/twy) changes in response to chronic progressive spinal cord compression: implications for human cervical compressive myelopathy. *PLoS One* [Internet]. 2013;8(5):e64528–e64528. Available from: <https://pubmed.ncbi.nlm.nih.gov/23717624>
79. Sakamoto M, Hosoda Y, Kojimahara K, Yamazaki T, Yoshimura Y. Arthritis and ankylosis in twy mice with hereditary multiple osteochondral lesions: With special reference to calcium deposition. *Pathol Int* [Internet]. 1994;44(6):420–7. Available from: <https://doi.org/10.1111/j.1440-1827.1994.tb01705.x>
80. Kubota M, Kobayashi S, Nonoyama T, Shimada S, Takeno K, Miyazaki T et al. Development of a Chronic Cervical Cord Compression Model in Rats: Changes in the Neurological Behaviors and Radiological and Pathological Findings. *J Neurotrauma* [Internet]. 2011;28(3):459–67. Available from: <https://doi.org/10.1089/neu.2010.1610>
81. Lee J, Satkunendrarajah K, Fehlings MG. Development and Characterization of a Novel Rat Model of Cervical Spondylotic Myelopathy: The Impact of Chronic Cord Compression on Clinical, Neuroanatomical, and Neurophysiological Outcomes. *J Neurotrauma* [Internet]. 2012;29(5):1012–27. Available from: <https://doi.org/10.1089/neu.2010.1709>
82. Karadimas SK, Klironomos G, Papachristou DJ, Papanikolaou S, Papadaki E, Gatzounis G. Immunohistochemical Profile of NF- κ B/p50, NF- κ B/p65, MMP-9, MMP-2, and u-PA in Experimental Cervical Spondylotic Myelopathy. *Spine (Phila Pa 1976)* [Internet]. 2013;38(1):4–10. Available from: <https://doi.org/10.1097/brs.0b013e318261ea6f>
83. Zhang M, Liu Q, Meng H, Duan H, Liu X, Wu J, et al. Ischemia-reperfusion injury: molecular mechanisms and therapeutic targets. *Signal Transduct Target Ther*. 2024;9(1):12.
84. Xia Y, Zhu J, Yang R, Wang H, Li Y, Fu C. Mesenchymal stem cells in the treatment of spinal cord injury: mechanisms, current advances and future challenges. *Front Immunol*. 2023;14:1141601.
85. Vawda R, Badner A, Hong J, Mikhail M, Lakhani A, Dragas R, et al. Early intravenous infusion of mesenchymal stromal cells exerts a tissue source Age-Dependent beneficial effect on neurovascular integrity and neurobehavioral recovery after traumatic cervical spinal cord injury. *Stem Cells Transl Med*. 2019;8(7):639–49.
86. Matsushita T, Lankford KL, Arroyo EJ, Sasaki M, Neyazi M, Radtke C, et al. Diffuse and persistent blood-spinal cord barrier disruption after contusive spinal cord injury rapidly recovers following intravenous infusion of bone marrow mesenchymal stem cells. *Exp Neurol*. 2015;267:152–64.
87. Morita T, Sasaki M, Kataoka-Sasaki Y, Nakazaki M, Nagahama H, Oka S, et al. Intravenous infusion of mesenchymal stem cells promotes functional recovery in a model of chronic spinal cord injury. *Neuroscience*. 2016;335:221–31.
88. Wang Z, Fang B, Tan Z, Zhang D, Ma H. Hypoxic preconditioning increases the protective effect of bone marrow mesenchymal stem cells on spinal cord ischemia/reperfusion injury. *Mol Med Rep*. 2016;13(3):1953–60.
89. Sanchez-Diaz M, Quiñones-Vico MI, de la Sanabria R, Montero-Vilchez T, Sierra-Sánchez A, Molina-Leyva A et al. Biodistribution of mesenchymal

- stromal cells after administration in animal models and humans: A systematic review. *J Clin Med*. 2021;10(13).
90. de Haro J, Zurita M, Ayllón L, Vaquero J. Detection of ¹¹¹In-oxine-labeled bone marrow stromal cells after intravenous or intralesional administration in chronic paraplegic rats. *Neurosci Lett*. 2005;377(1):7–11.
91. Paul C, Samdani AF, Betz RR, Fischer I, Neuhuber B. Grafting of human bone marrow stromal cells into spinal cord injury: a comparison of delivery methods. *Spine (Phila Pa 1976)*. 2009;34(4):328–34.
92. Wang W, Huang X, Lin W, Qiu Y, He Y, Yu J et al. Hypoxic preconditioned bone mesenchymal stem cells ameliorate spinal cord injury in rats via improved survival and migration. *Int J Mol Med [Internet]*. 2018;42(5):2538–50. Available from: <https://pubmed.ncbi.nlm.nih.gov/30106084>
93. Čížková D, Rosocha J, Vanický I, Jergová S, Čížek M. Transplants of Human Mesenchymal Stem Cells Improve Functional Recovery After Spinal Cord Injury in the Rat. *Cell Mol Neurobiol [Internet]*. 2006;26(7–8):1165–78. Available from: <https://doi.org/10.1007/s10571-006-9093-1>
94. Cizkova D, Novotna I, Slovinska L, Vanicky I, Jergova S, Rosocha J et al. Repetitive Intrathecal Catheter Delivery of Bone Marrow Mesenchymal Stromal Cells Improves Functional Recovery in a Rat Model of Contusive Spinal Cord Injury. *J Neurotrauma [Internet]*. 2011;28(9):1951–61. Available from: <https://doi.org/10.1089/neu.2010.1413>
95. Kurihara K, Sasaki M, Nagahama H, Obara H, Fukushi R, Hirota R, et al. Repeated intravenous infusion of mesenchymal stem cells enhances recovery of motor function in a rat model with chronic spinal cord injury. *Brain Res*. 2023;1817:148484.
96. Dos Santos Ramalho B, Marques Pestana F, Andrade Prins C, Soares Dos Santos Cardoso F, Rufino Cavalcante D, de Augusto S et al. Effects of Different Doses of Mesenchymal Stem Cells on Functional Recovery After Compressive Spinal-Cord Injury in Mice. *Neuroscience*. 2019;400:17–32.
97. Crisan M, Yap S, Casteilla L, Chen CW, Corselli M, Park TS, et al. A perivascular origin for mesenchymal stem cells in multiple human organs. *Cell Stem Cell*. 2008;3(3):301–13.
98. Kurtz A. Mesenchymal stem cell delivery routes and fate. *Int J Stem Cells*. 2008;1(1):1–7.
99. Nakazaki M, Yokoyama T, Lankford KL, Hirota R, Kocsis JD, Honmou O. Mesenchymal stem cells and their extracellular vesicles: therapeutic mechanisms for Blood-Spinal cord barrier repair following spinal cord injury. *Int J Mol Sci*. 2024;25(24).
100. Andreotti JP, Silva WN, Costa AC, Picoli CC, Bitencourt FCO, Coimbra-Campos LMC, et al. Neural stem cell niche heterogeneity. *Semin Cell Dev Biol*. 2019;95:42–53.
101. Giachino C, Taylor V. Notching up neural stem cell homogeneity in homeostasis and disease. *Front Neurosci*. 2014;8:32.
102. Dulken BW, Leeman DS, Boutet SC, Hebestreit K, Brunet A. Single-Cell transcriptomic analysis defines heterogeneity and transcriptional dynamics in the adult neural stem cell lineage. *Cell Rep*. 2017;18(3):777–90.
103. Fu L, Zhu L, Huang Y, Lee TD, Forman SJ, Shih CC. Derivation of neural stem cells from mesenchymal stemcells: evidence for a bipotential stem cell population. *Stem Cells Dev*. 2008;17(6):1109–21.
104. Changmeng Z, Hongfei W, Cheung MCH, Chan YS, Shea GKH. Revealing the developmental origin and lineage predilection of neural progenitors within human bone marrow via single-cell analysis: implications for regenerative medicine. *Genome Med*. 2023;15(1):66.
105. Oliveri RS, Bello S, Biering-Sørensen F. Mesenchymal stem cells improve locomotor recovery in traumatic spinal cord injury: systematic review with meta-analyses of rat models. *Neurobiol Dis*. 2014;62:338–53.
106. Shang Z, Wang R, Li D, Chen J, Zhang B, Wang M, et al. Spinal cord injury: A systematic review and network Meta-Analysis of therapeutic strategies based on 15 types of stem cells in animal models. *Front Pharmacol*. 2022;13:819861.
107. Pischietta F, D'Amico G, Dander E, Biondi A, Biagi E, Citerio G, et al. Immunosuppression does not affect human bone marrow mesenchymal stromal cell efficacy after transplantation in traumatized mice brain. *Neuropharmacology*. 2014;79:119–26.
108. Youseffard M, Nasirinezhad F, Shardi Manaheji H, Janzadeh A, Hosseini M, Keshavarz M. Human bone marrow-derived and umbilical cord-derived mesenchymal stem cells for alleviating neuropathic pain in a spinal cord injury model. *Stem Cell Res Ther*. 2016;7:36.
109. Sammal E, Alia C, Vegliante G, Colombo V, Giordano N, Pischietta F, et al. Intravenous infusion of human bone marrow mesenchymal stromal cells promotes functional recovery and neuroplasticity after ischemic stroke in mice. *Sci Rep*. 2017;7(1):6962.
110. Yang C, Wang G, Ma F, Yu B, Chen F, Yang J, et al. Repeated injections of human umbilical cord blood-derived mesenchymal stem cells significantly promotes functional recovery in rabbits with spinal cord injury of two non-continuous segments. *Stem Cell Res Ther*. 2018;9(1):136.

Publisher's note

Springer Nature remains neutral with regard to jurisdictional claims in published maps and institutional affiliations.